



**CÁMARA DE PRUEBAS PARA CCD EN
DAMIC-M/LSM
(CCD Test Chamber Setup for DAMIC-M/LSM)**

**Trabajo de Fin de Máster
para acceder al**

**MÁSTER EN FÍSICA DE PARTÍCULAS Y DEL
COSMOS**

Autor: Darío González Herrera

**Director\es: Dra. Rocío Vilar Cortabitarte
Codirector: Dra. Julia Mónica Campa Romero**

Septiembre - 2022

Acknowledgements

Gracias a mi familia que sin su apoyo incondicional no hubiera realizado este trabajo de fin de máster, además de apoyarme cada quien a su modo para seguir adelante en mi carrera y han sido mi inspiración y motivación en cada paso de mi vida.

También quiero agradecer a mi directora y codirectora de TFM, de ambas personas me llevo lo mejor de mi estancia en la Universidad de Cantabria y sus consejos para los siguientes pasos en mi carrera.

Esta experiencia de estudiar en España la he tenido gracias a la Fundación Carolina que me dió la oportunidad de conocer a mis amigos Luis, Sonia, Paola, Efrén, Anub y Cristian que me ayudaron mucho en momentos complicados de mi estancia y les agradezco su resiliencia conmigo.

Finalmente, quiero agradecer a mis profesores de la Universidad de Cantabria que han sido muy amables y generosos de compartir su motivación, conocimiento y dedicación por la ciencia a través de sus clases y asesorías académicas .

Abstract

The search for non luminous matter is demanding to have better sensitivity for the direct Dark Matter detection. On this path, the Institute of Physics in Cantabria has installed within its facilities a CCD Test Chamber aiming to calibrate and measure the dark current in skippers CCDs to decrease the noise level for the DAMIC-M experiment. In this final master project I describe some basics on skipper CCDs, the Ironman CCD Test Chamber components, the LEACH system, the Slow Control and a I give a brief analysis on the cryostat performance and the first CCD images taken in the Clean Room.

Keywords: Dark Matter, Rotation Curves, WIMPs, Skipper CCD, Cryostat, readout noise, LEACH system and Slow Control.

Resumen

La búsqueda de materia no luminosa exige una mejor sensibilidad para la detección directa de Materia Oscura. En este rubro, el Instituto de Física de Cantabria ha instalado dentro de sus instalaciones una Cámara de Pruebas para CCD's con el objetivo de calibrar y medir la corriente oscura de los skippers CCDs con la intención de disminuir el nivel de ruido en el experimento DAMIC-M. En este Trabajo de Fin de Máster, describo algunos conceptos básicos sobre los skipper CCDs, los componentes de la cámara de prueba Ironman para CCDs, el sistema LEACH y el Slow Control, además de realizar un análisis del rendimiento del criostato así como de las primeras imágenes de CCD tomadas en la sala limpia.

Keywords: Materia Oscura, Curvas de rotación, WIMPs, Skipper CCD, criostato, ruido de lectura, sistema LEACH y Slow Control.

Contents

1	Brief review about Dark Matter	6
1.1	Introduction	6
1.2	Rotation Curves of Spiral Galaxies	6
1.3	Gravitational Lensing	7
1.4	Features for Dark Matter candidates	10
2	DAMIC-M Experiment.	11
3	Charge Coupled Devices for Direct Dark Matter Detection in DAMIC-M	14
3.1	Operation	15
3.2	Performance Functions	17
3.2.1	Charge Generation	17
3.2.2	Charge Collection	17
3.2.3	Charge Transfer	18
3.2.4	Charge Measurement	18
3.3	Noise Sources in a CCD Image	19
3.3.1	Readout Noise	19
3.3.2	Dark Current	19
3.3.3	Luminescence	20
3.3.4	Cosmic Rays	21
3.4	Skipper CCD	21
3.4.1	Operation	22
3.4.2	Background Performance	25
4	Test Chamber Setup for CCD's.	26
4.1	Cryostat	26
4.1.1	Equipment for Ironman	28
4.1.2	Cryogenic System	28
4.1.3	Operation	33
4.1.4	Performance	34
4.2	LEACH System	36
4.3	Slow Control	42
4.3.1	Software	42
4.3.2	Hardware	44

5	First skipper CCD images at IFCA	46
6	Conclusions	49
7	Bibliography	50

Motivation

The existence of non luminous matter is been a big mystery since many decades ago [1]. Its evidence at cosmological scale has caused a very intense search in several forefront experiments all over the world aiming to find hints of its quantum nature. Over the years, the scientist have understood and discovered all particles predicted by the Standard Model of Particle Physics. All this could not be possible without the development of some of the most stunning and brilliant experiments involving very innovative techniques at the moment since particle detectors as the cloud chamber to very huge particle colliders that have allowed us to do a step forward in looking for physics beyond the Standard Model then the searches for Dark Matter (DM) candidates will drive the development of new technologies at very high sensitivity and very low noise levels.

One of these efforts are being performed by the DAMIC-M collaboration [2], specially in the development of the new generation of skipper CCDs with the purpose to build a Kg size skipper CCD detector for direct Dark Matter detection that at least will give new heights for some DM candidates. On this path, the Institute of Physics in Cantabria (IFCA) is installing a CCD test chamber in its facilities to do several characterizations of skipper CCD devices and help to improve the dark current and noise levels in CCDs.

In the first chapter, this final project will review briefly the present knowledge about the Dark Matter from the most relevant evidence to the expected characteristics for DM candidates. In the second chapter, I described the DAMIC-M experiment and the sensibility for different DM candidates. Then, in the third chapter, the main features in the CCD characterization are introduced as well as the new characteristics for skipper CCDs. For the Fourth chapter, I presented the main components of the CCD Test chamber installed in the last semester at the IFCA facilities together with an initial and basic optimization of the parameters to read the CCDs. In the fifth chapter, some first CCD measurements are described and finally in the sixth chapter the conclusions on the CCD test chamber performance, operation and the first measurements are discussed.

1 Brief review about Dark Matter

1.1 Introduction

In the 19th century occurred the first evidence of what we identify as Dark Matter when Bessel measured the position of Sirius and Procyon and concluded that each one was in an orbit with an invisible object with a similar mass [1]. After that, in 1933, the Swiss astronomer Fritz Zwicky while he was studying the Redshift of extra galactic nebulae he applied the Virial theorem to the Coma cluster in order to estimate the dispersion velocity and discovered that there must be a density mass about 400 times greater than the observed luminous mass in the system [3]. These are some of the most relevant initial hints for the existence of what we call as Dark Matter now.

Trough this chapter I aim to explain some of the most relevant evidences for the existence of Dark Matter and the current experiments searching for it .

1.2 Rotation Curves of Spiral Galaxies

It was until the 60's, 70's and 80's when the astrophysicist Vera Rubin, Kent Ford, and Ken Freeman published their famous rotation curves on spiral galaxies that provided more accurate evidence of the existence of Dark Matter in the outskirts of several galaxies [4] [5].

In their research, they observed how the rotation curves of some spiral galaxies are almost constant in the halo showing the need for a invisible matter existence.

Studies of the dynamics of the spiral galaxies have been taken from optical observations and radio hydrogen 21 cm band emission. With the optical observations was possible determine the rotational velocity across the nucleus and inner regions while radio 21 cm line light is capable to penetrate the dust clouds from the galaxy halo. From this measurements the researchers can compare the structure and dynamics between galaxies and determine with certain accuracy the position of our Solar System within the Milky Way.

One usual approach is if we do assume equilibrium between the gravitational force due to the integral mass and the centrifugal force on a punctual

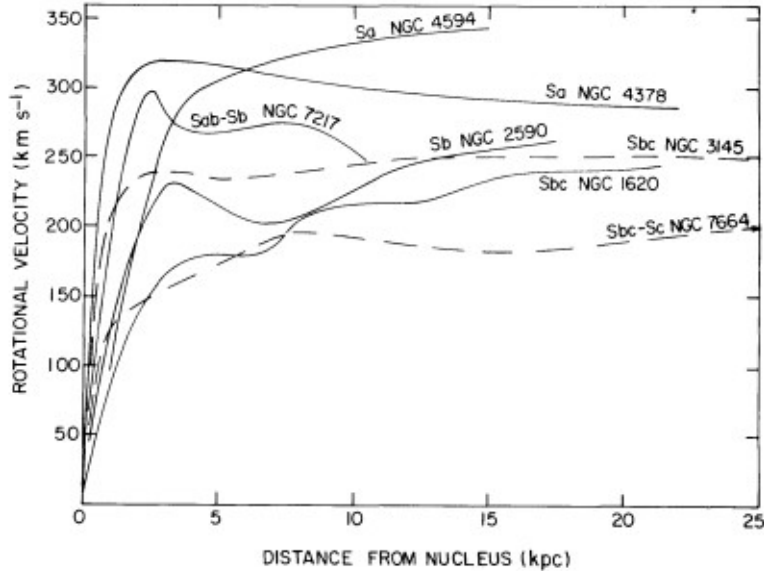


Figure 1: Rotation curves of seven spiral galaxies as a function of distance from Nucleus, it is possible to observe its flat behavior, some of them with pronounced spikes due to they are Early-type galaxies [6]

body located in the arms of the galaxy we obtain:

$$v(r) = \sqrt{\frac{GM_{int}}{r}} \quad (1)$$

Clearing for M_{int} and with $v(r) \approx const$:

$$M_{int} = const \cdot r \quad (2)$$

therefore we can expect a lineal behaviour for the integral mass distribution and this is very approximately to the observed profile of the integral mass as shown in the figure 2.

1.3 Gravitational Lensing

More than one hundred years ago, Eddington and a very talented group of astronomers confirmed the Einstein's General Relativity theory by detecting the tiny gravitational lensing of the Sun's gravitational field by taking advantage of a solar eclipse in the southern hemisphere [7]. Now, this effect is

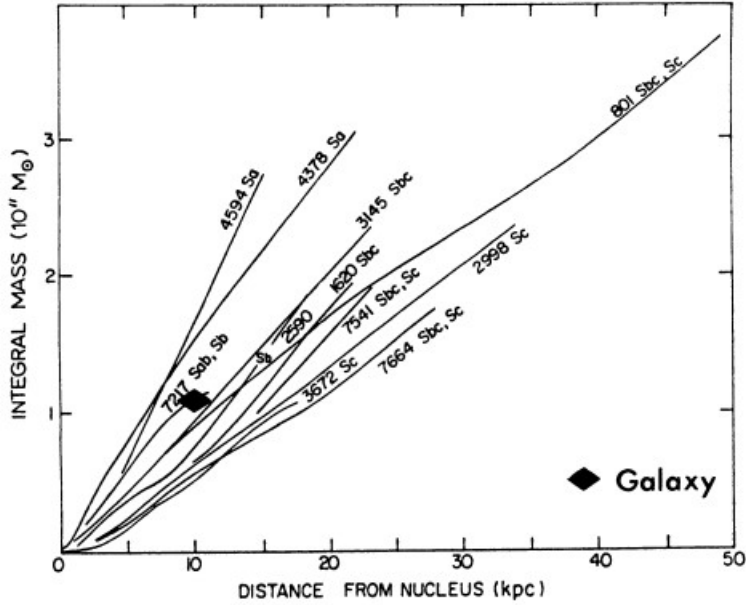


Figure 2: Integral mass within a disk of radius r , as a function of r . These observations prove the linear behaviour for spiral galaxies[6].

been used to explore several astronomical objects such that Galaxy Clusters, exoplanets, MACHOS, Black Holes and even the Dark Matter in Galaxy Halos [8].

From the General Relativity theory, Einstein argued that the deflection of photons as they pass through the warped spacetime of a gravitational field could exist [9] we call it as Gravitational Lensing. This phenomenon can cause a shifting, distortion and magnification of images of the background objects as galaxies or Clusters [10]. Now studying this deflected light could provide information about the constraints on the mean density of dark matter, and its density relative to baryonic matter; the size and mass of individual dark matter particles as well as its cross section under various fundamental forces [11].

In the figure 3 the gravitational effect on light is shown and classified according to deformation in the shape of a spherical light source while in the figure 4 shows the baryonic and DM distribution in a sky section.

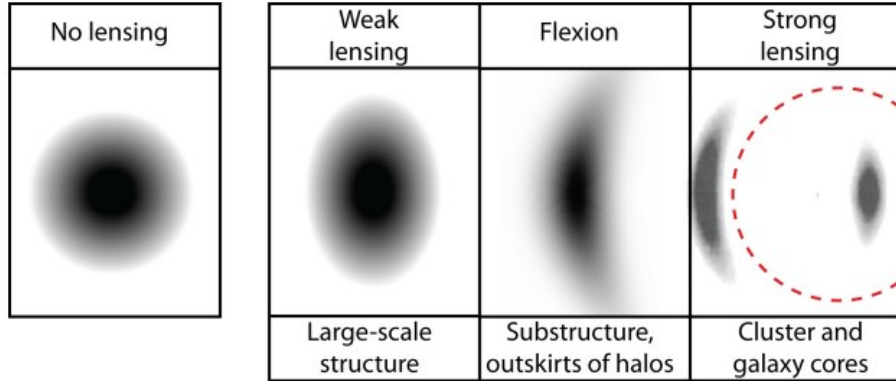


Figure 3: This image [11] shows the estimate figure that an observer would detect from a bright circular source which light passes through different intensity gravitational field. In weak lensing the circular object is seen as an ellipse. For stronger gravitational fields the light line forms a flexion around the massive object. For very massive objects like galaxy clusters the deflected light can be divided and it could form many images (Strong lensing).

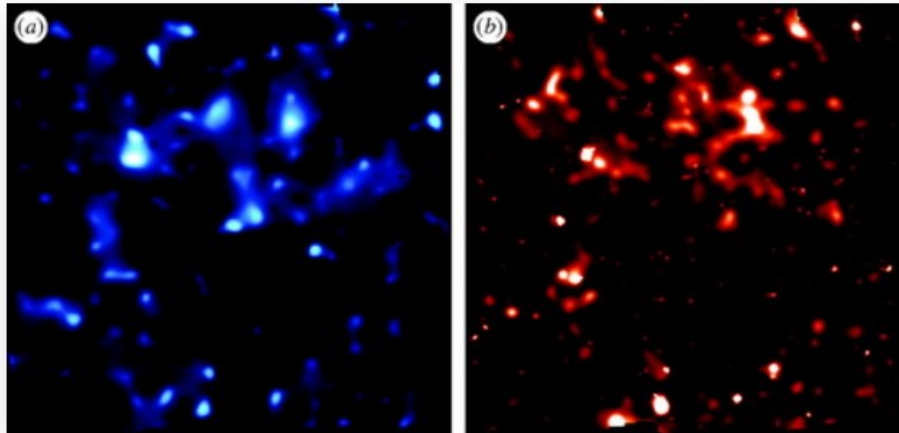


Figure 4: In these two images [12] we can compare the distribution of Dark Matter (inferred by using weak gravitational lensing with light from background galaxies from the COSMOS survey [13]) and its equivalent for baryonic matter distribution.

1.4 Features for Dark Matter candidates

From the Planck and WMAP missions the estimation for the baryon density $\Omega_b \approx 0.045$ and the dark matter density $\Omega_{dm} \approx 0.2$ by the precise observations of the Cosmic Microwave Background (CMB) spectrum of density fluctuations and its baryon acoustic oscillations [14], [15]. The difference between these two densities is very big and it has been a motivation for the search of DM since by using spatial telescopes to underground detectors.

Although there is not a confirmed Dark Matter particle discovery there are some constraints that may all DM candidates must accomplish [16]:

- **Non-interacting nature:** This is suggested by considering when two clusters collide no evidence of interaction between DM is observed.
- **Stable:** Due to the non-interacting nature of the DM with itself this suggests it must remain the same amount since the beginning of the universe formation thus the DM lifetime must be larger than the age of the universe.
- **Non-Relativistic:** In the current standard cosmological model Λ CDM the structure formation grows hierarchically suggesting that the DM is cold (CDM). Also at large scales the CDM agrees with the structure formation.
- **Non-Baryonic:** From the CMB observations and big bang nucleosynthesis the baryonic matter density is very low in the universe thus the rest of the matter density is made up of DM.
- **Massive:** The paradigm about CDM is that it is mostly made of Weakly Interacting Massive Particles (WIMPs). Furthermore, the WIMPs include any non-baryonic massive particle that interacts with any interaction that is either weak or sub-weak. This hypothetical particle arises from many proposed models and currently is very one of the most promising theories because a large fraction of their typical detection rates are within reach of current or planned detectors [17].

Additionally, there is a number of proposed solutions (at least partially) to CDM besides the WIMPs, for instance, MACHOs, light gravitinos, hidden dark matter, sterile neutrinos, and axions [18].

2 DAMIC-M Experiment.

Currently, the The DArk Matter in CCDs at Mondane (DAMIC-M, for short) experiment is an international collaboration between partners in America and Europe aiming to improve the CCDs technology and techniques for detection of nuclear and electronic recoils induced by dark matter particles in the silicon bulk [19]. The DAMIC-M collaboration is a continuity of the DAMIC experiment which uses the scientific CCDs located in underground inside the SNOLAB's facilities [30].

At the beginning, the main purpose for DAMIC was searching for Weakly-Interacting Massive Particles (WIMP) which induce nuclear recoils of keV-scale energies [31] afterwards over the years of taking data new upper limits on the cross-section for WIMPs below $4 \text{ GeV}/c^2$ were reached [32] and new improvements in reducing the dark current, relatively low mass of the silicon nucleus as well as using high resistivity silicon materials in CCDs appeared to go further into the search for Dark photon and another candidates from the hidden sector (see figure 5) [33].

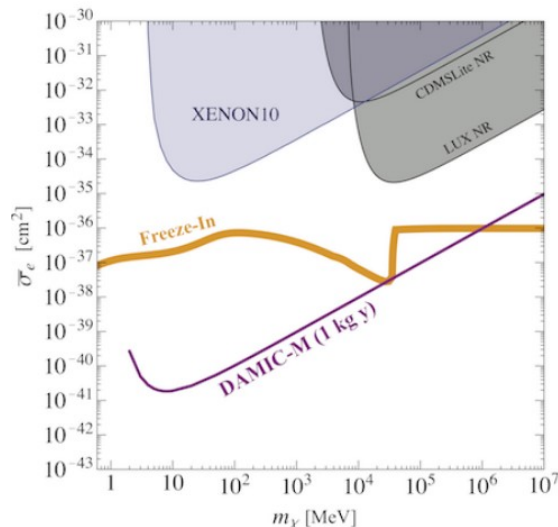


Figure 5: In this plots, we observe in purple the forecast for the DM-electron cross section in the new DAMIC-M measurements, enough to exclude the hypothesis that all DM in the universe is made of dark photons (orange).

For DAMIC-M, the skipper CCDs material will provide a new target for

electron recoils produced by Dark Matter particles and Silicon nuclei. In incoming years as part of the experiment it is expected to install a new skipper CCDs module of the order of Kg size, a magnitude bigger than the last one planned with 100 g for the SENSEI experiment [36].

This new experiment will be located in the Laboratoire Souterrain de Modane (LSM) [34] at 1700 m underground very near to the French-Italian border. This will shield the detector from the cosmic and atmospheric radiation (external noise for CCD images). Furthermore, the facilities in this laboratory allows to perform detector packaging, test and assembly underground as well as supplying radon-free air inside contributing to minimize surface backgrounds.

The proposed prototype for DAMIC-M in figure 6 is composed by a cryostat vessel that keep the CCDs in its optimal temperature, all this is inside a box surrounded by infrared (IR) shields. Cooling is transmitted from a liquid nitrogen dewar located outside the shielding trough a copper cold finger. Due to standard lead contains some ^{210}Pb nucleus (which chain products may generate penetrating bremsstrahlung photons escaping the shield) and that a 20 cm thick lead encloses the cryostat then an ancient lead recovered from a Roman ship sunk in Brittany in 400 A.C. compose the 5 cm innermost shield. The entire lead shield is enclosed by 40-cm-thick polyethylene to efficiently stop external neutrons.

As one can imagine, the background sources in laboratory is always a big problem at the time to calibrate and perform the best possible measurements. From the experience in DAMIC at SNOLAB the most relevant backgrounds are:

- **Cosmogenic tritium:** Radioactive isotopes are produced via cosmogenic activation in detectors and other materials, particularly tritium has a long very low endpoint energy, long half-life and it can be generated in any material as a spallation product [35]. The precautions to be taken are minimize exposure to cosmic rays with shielding during transport/fabrication; CCD packaging and test underground at LSM. Also, R&D ongoing to evaluate tritium removal by wafers/CCDs baking.
- **Surface ^{210}Pb :** this can be attenuated by minimizing exposure to radon. Also by using ancient lead shields.

- **Radiogenic background:** It is possible to have some nuclear reactions underground coming from the own material used in the experiment interacting with the environment. To reduce the signals that can block the DM detection, it is so useful to utilize electro formed copper in many components of the DAMIC-M setup.

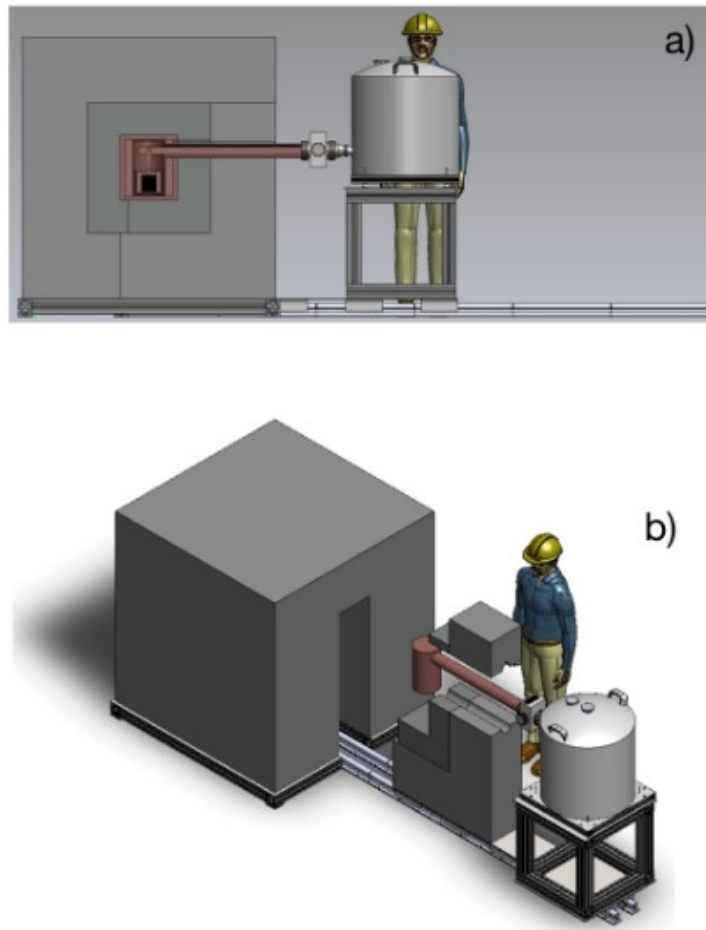


Figure 6: This pictures shows the prototype for the DAMIC-M experiment at LSM. a) Cross-sectional view of the chamber containing the CCDs. b) This image shows the rails by which the different parts of the interior of the chamber are disassembled.

3 Charge Coupled Devices for Direct Dark Matter Detection in DAMIC-M

Reminding that part of the purpose of this final master project is introduce the first images with skipper CCDs in the clean room at IFCA it is necessary to have some basic concepts about the Charge Coupled Devices working. In this chapter, I start explaining the basic concept, the bias voltages, materials, noise sources and readout mechanism in a CCD. After that, I explain how the functionality of a skipper CCD came up and its advantages in the search of Dark Matter with DAMIC-M.

During the last decades, the CCDs have been one of the most important tool in astronomical observations from gamma rays to radio waves [20]. They have been used in grounded and spatial observatories due to its high capacity to collect ionized charge produced by the photoelectric effect and sensitivity hundreds of times greater than film. The CCD was invented in October 19, 1969, by Willard S. Boyle and George E. Smith at Bell Telephone Laboratories aiming to develop a new memory device combining some principles of the magnetic bubble memory and diode arrays in silicon then this raised problems with charge storage in individual diodes. After the publication of the three phase mechanism for charge transfer and the CCD concept; a new idea appeared: a CCD could be used for imaging using linear and array areas.

A simple CCD is a two dimensional grid composed by a number of metal oxide semiconductor (MOS) pixels. Each MOS capacitor has a depletion region where the ionization charge caused by an incident particle is stored. After that, by putting together these capacitors to others (pixels) and by managing the voltages at the capacitor gates, the charge is moved to the amplifier to be read.

3.1 Operation

A particle interacting with the silicon nucleus or the electron generates an electron-hole that moves along the electric field created with the bias voltage applied. Potential wells are creating to collect the electrons or the holes that have not been recombined in the lattice [21]. these charged remains in these wells until move to the serial register therefore the charge readout is performed by reading column by column (or row by row) pixels.

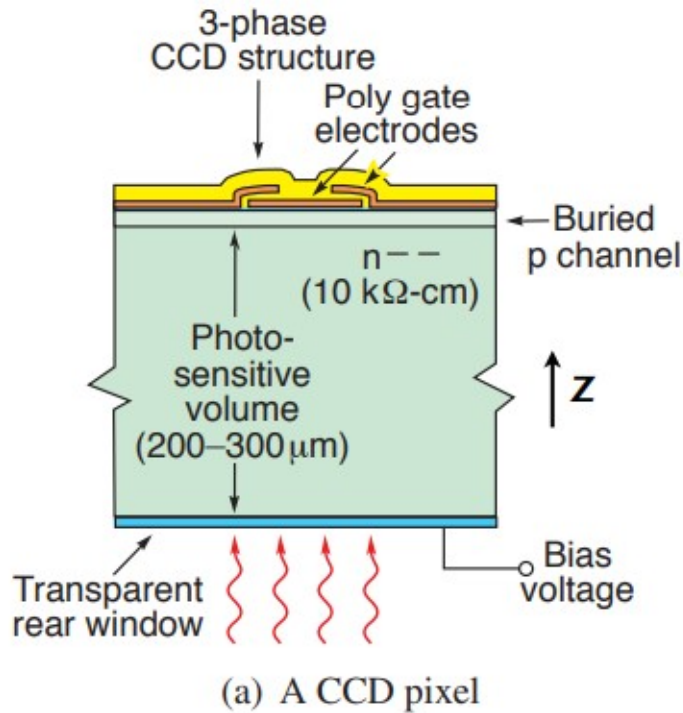


Figure 7: Cross-sectional diagram of a typical $15 \mu m \times 15 \mu m$ pixel in CCD used in DAMIC experiment [22]. The high resistivity in this CCD goes from 10000 to 12000 $\Omega\text{-cm}$ [23].

The figure 7 shows the architecture of a CCD pixel, in essence a pixel is made up of a $p - n$ junction so there are drift and diffusion electrons and holes that can be recombined by a depletion voltage V_{sub} creating a bulk area where the particles interact with the semiconductor material. In three phase clock CCD, the idea is create potential wells to move the collected charge

inside the pixel and transport it to the next pixel row as it is shown in the figure 8:

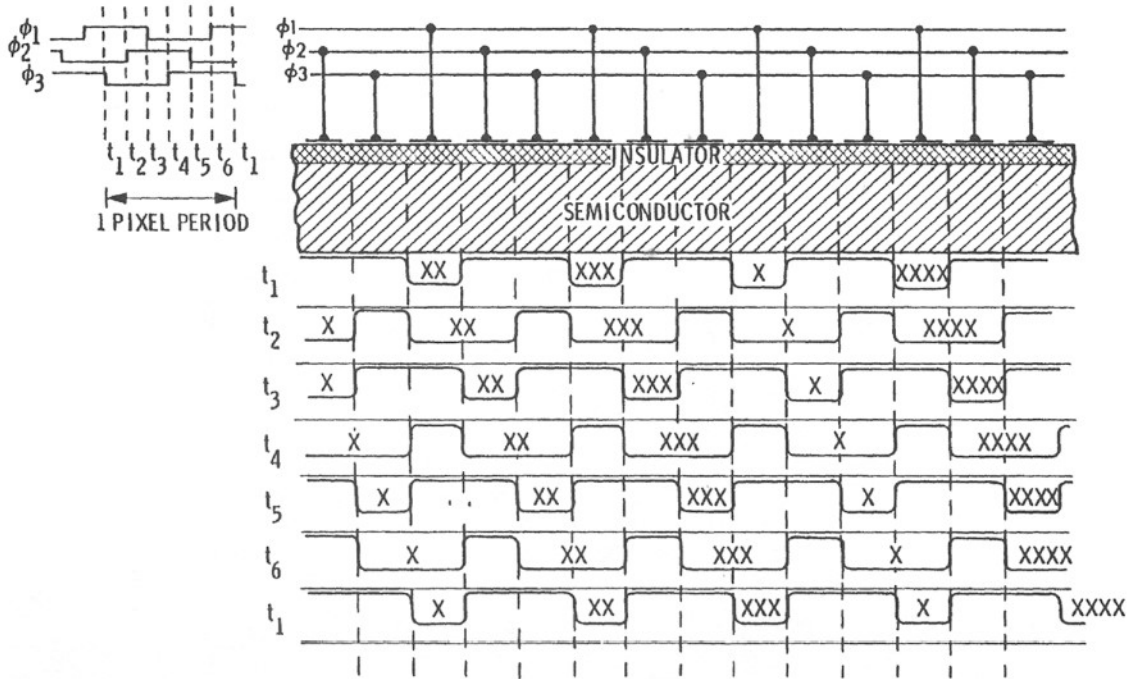


Figure 8: This figure show how the ϕ_1 , ϕ_2 and ϕ_3 clocks are high or low in order to move the collected electrons column by column [24] or row by row (according to the case).

The order in clock activation make that the charge goes backwards, this characteristics is beneficial in some CCD applications. Some CCD seem very robust and it is unlikely to cause some mechanical damage but remembering that there are logical gates in the pixels it highly recommended to prevent any static discharge.

Another thing to take into account is that depending on the direction of the incident particles, it is said that a CCD is front-illuminated or back-illuminated. This classification is useful at the time to consider better result due to in front-illuminated devices the particles interact with the gate structure losing some of their initial energy while in a back-illuminated device the particles interact with the sensitive area. At the end, the circumstances of

the experiment is the main reason to decide between this two architectures.

3.2 Performance Functions

This section is dedicated to give some introduction to some of the basic functions that a CCD must perform in order to yield an image. They are four functions: charge generation, charge collection, charge transfer and charge measurement [24].

3.2.1 Charge Generation

This is a very relevant feature in CCDs used for photon detection because the material properties in the depletion area determine how good is the pixel to generate a pair (sometimes are pair) of electron-hole for a incident photon with specific energy. This phenomena is explained by the photoelectric effect and is described by the Quantum Efficiency (QE) function which is the fraction of incident photons that produce a sufficient electric charge to be detected. Moreover, the QE depends in the wavelength of the incident photons and then it is necessary that this photons have a higher energy than the band gap of the silicon material if not the the device is transparent.

Due to the band gap of the Silicon material depends on the temperature (it reduces at lower temperatures) also determines the QE so when the band gap is lower the QE changes towards new wavelengths.

3.2.2 Charge Collection

Another characteristic for CCD performance is how well the device is capable to create an image from the electrons generated. Mainly we can determinate this characteristic by using three parameters: the area or number of pixels contained on the chip, the number of signal electrons that a pixel can hold and the ability of the "target pixel" to efficiently collect electrons when they are generated.

Explaining in more detail each of the three parameters above is very complex and it is out of purpose in this final project but we can standout some relevant considerations for the CCD architecture. The size of a pixel is proportional to the number of electrons to be stored, for scientific CCD

this number is about 200 000 electrons [24] but it is necessary to reach an equilibrium between the size and number of pixel in a device because also having a high concentration of pixels the amount of data, the costs and the readout time are also significantly incremented. This is the reason why some CCD manufactures incorporate many amplifiers in chip.

3.2.3 Charge Transfer

As exposed before, the generated charge in each pixel have to move on until it gets to the CCD serial register hence the importance to keep almost intact every charge packet transferred. Even having a 99% of transferred charge after 100 transfers only 63% of the initial charge is conserved. Currently, for scientific CCD a charge transfer efficiency about 99,9999% is reached [24] what means that only one electron is lost by one million of transferred electrons.

Some factors that determine the charge transfer efficiency are fringing fields between phases, thermal diffusion, and self-induced drift. A special consideration for CCD is that not all the pixels do the well the same performance and it is possible to have some defects in images. Even there are some bulk traps caused by impurities or lattice defects within the silicon that absorb some electrons, the number of traps can be reduced by building chips with the best silicon material available [24].

3.2.4 Charge Measurement

One major final step for CCD imaging is detecting and measuring the charge in each pixel. To do this duty, the collected charge is pushed into a small capacitor connected to an output MOSFET amplifier. For each pixel this output amplifier generates a voltage proportional to the collected charge yielding a respectable signal for digital conversion.

An important factor is reduce as much as possible the noise in the MOSFET amplifier because the CCD sensitivity depend on. Nevertheless, this fundamental noise source can not be completely reduced since it is generated by the random fluctuations in the current that flows through the transistor. At the beginning this noise was about $30 e^-$ rms but today this noise is below $1 e^-$ rms [24].

3.3 Noise Sources in a CCD Image

Unfortunately, there is several noise sources in chip as well from different electronics connected or surrounding the CCD but this chapter will give a number of noises that motivate the CCD Test Chamber setting since the idea is help us to characterize some of this noises.

3.3.1 Readout Noise

In a practical way to refer with Readout Noise is the number of electrons introduced per pixel into the final signal upon readout of the device, mainly it is caused by the output amplifier or another element in the readout electronics [25].

One component for this noise is the conversion from an analog signal to a digital number, which is not perfectly repeatable that means not always the electronics reads the same value for the collected charge despite of measuring the same charge packet. The other component is the noise coming from the electronics into the entire process introducing electrons which yield random fluctuations in the output. The average level of this two components (after summing them) is the readout noise and is limited by the output electronic properties [25].

In the output image, the readout noise is added to the collected charge in every pixel [25].

3.3.2 Dark Current

The Dark Current is an intrinsic characteristic of the semiconductors. It is the measured charge produced by thermal random creation of minority carriers even when there is no light interacting with the material hence the name. When the thermal agitation is high enough, electrons will be freed from the valence band and become collected within the potential well of a pixel adding more charge to the output signal [25]. This noise can be attenuated in a good portion by reducing the device temperature [29]. From all the area where the dark current comes from, the contribution from surface states is the dominant [24].

Mainly the dark current depends on the CCD temperature but also it has a dependence upon the properties of the used material which can be overshadowed by reducing the impurities in Silicon and surfaces materials [25].

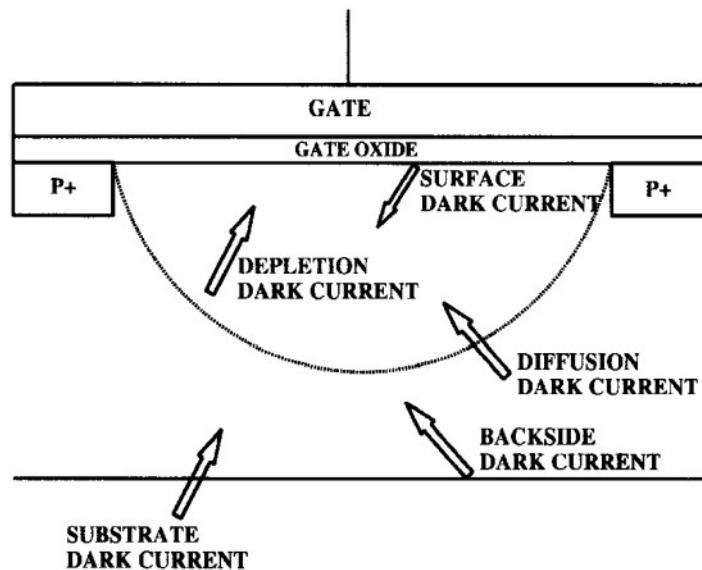


Figure 9: This image show different areas inside a single silicon pixel that produce the more significant dark current amounts.

3.3.3 Luminescence

Besides the luminescence in the output amplifier, there is some kind of this noise in the clocking system and pixels.

In case of the Clocking, luminescence appears by simply clocking the gates, particularly it is very common in CCDs fabricated with a SiO_2 gate insulator but dual insulating systems appear to not undergo this problem. The best explanation to this phenomena is that when the clock signals generate some electrons in the gate insulator with the enough energy to produce infrared photons which can be detected by the neighboring pixels in the vertical section [24].

The pixels luminescence is one of the biggest problems for CCD design since it can add a high noise to the neighboring pixels. Also it can add charge when the collected electrons in the capacitor are moving so in we observe in the output image some large lines and luminous pixel clusters. The problem could be explained by a high clock voltage which can over-stress the gate insulator. The best option to do in this cases is replace the CCD because there is not a solution or improvement so far. This pixels can appear under normal operation conditions and without replacing the CCD it will only turn worse [24].

3.3.4 Cosmic Rays

The secondary events from a collision between a cosmic ray and particles in the Earth's atmosphere can be detected in a CCD. Moreover it is very likely to see muons and electrons in an output image such that they become a very important background when the purpose is to detect dark matter. Therefore it is necessary to blind the sensors by putting them underground. The cosmic rays are an external noise for the CCDs.

After a cosmic ray collision in the atmosphere, a chain reaction occurs, spreading out the creation of new particles (secondary particles). The width of this chain reaction as well as the particle flux are conditioned on the initial particle and its energy. Furthermore, the number of particles that a CCD can detect depends on the high (sea level) at which the setup is settled.

In an output image without shield, the muons are about 74%, electrons 25% and protons 1% [24]. They leave some tracks, each one is different due to the cross-section with the Silicon nuclei. Sometimes they could be enough energetic that can damage the pixels producing a irreversible injury to the CCDs.

3.4 Skipper CCD

As introduced before, there are several sources for noise in a CCD lecture but specially the readout noise is a background signal that can be treated with a relative new technology called skipper CCD. With this new improvement the limits for Dark Matter detection are reduced as well conserving a good

sensor deep which increase the probability for detection.

The idea behind the skipper CCD technology is perform a number N of charge measurements, each one with different values for read noise (RN). Then, take off the average for each pixel outside the sensor and take it as the output image. Trough this section some features about the skipper CCD as its architecture and performance are exposed.

3.4.1 Operation

In the case for DAMIC-M, the skipper CCDs are designed by the Lawrence Berkeley National Laboratory and it is expected to follow the layouts as described below [26]:

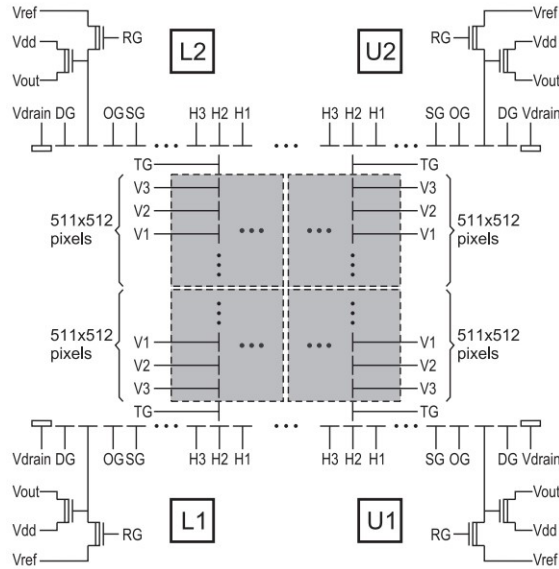


Figure 10: Scheme of the bias voltage for a skipper CCD designed in LNBL. For the new sensors generation some configuration could change like the number of pixels or the CCD size but the functionality is the same (Credits: Moroni).

In the figure 8, we can observe that the vertical clocks (V1,V2 and V3) and horizontal clock (H1,H2 and H3) are still present as the normal CCDs but the difference is that in the output amplifiers is installed a floating gate output. The floating gate is on charge of measuring the packet charge by coupling the signal electrons in the CCD channel and the current flow in the MOS transistor [27]. This technique take advantage of the very low noise and high resistivity in the CCD channel permitting to read in a non destructive way the number of electrons in each pixel.

TABLE I. Skipper CCD detector characteristics.

Characteristic	Value	Unit
Format	4126×866	pixels
Pixel scale	15	μm
Thickness	200	μm
Operating temperature	140	Kelvin
Number of amplifiers	4	
Dark current ^a	$<10^{-3}$	$e^-/\text{pixel}/\text{day}$
Readout time (1 sample)	10	$\mu\text{s}/\text{pixel}/\text{amp}$
Readout noise (1 sample)	3.55	$e^-_{\text{rms}}/\text{pixel}$
Readout noise (4000 samples)	0.068	$e^-_{\text{rms}}/\text{pixel}$

Figure 11: This table [28] expose some features about the current CCDs technology for the SENSEI experiment. It should be noted how the readout noise is reduced by two orders of magnitude when a 4000 charge samples are taken.

As it is explained in [26], the control of the current flux in the floating gate amplifier is carried out by the summing gate clock (SG), output gate clock (OG), dump gate clock (DG) and the timing of these signals for reading out the same pixel three times [26]. At t_0 , the packet charge is moved from H3 to SG. At the same time DG and the reset gate (RG) signals go down to remove the previous pixel charge from the channel and set the voltage in the pixel to the reference voltage V_{ref} . In t_1 the charge is transferred from the SG to the SN through the OG. By lowering voltage levels, in t_2 the holes are transferred backward again to the SG. After the charge is moved out from SN, in t_3 , the voltage in RG is set to V_{ref} which is a new reference voltage for

the new pixel sample. The pixel value is encoded by the difference between the high level (signal) and reference level (pedestal) in the video signal V_{video} as shown in the next figure.

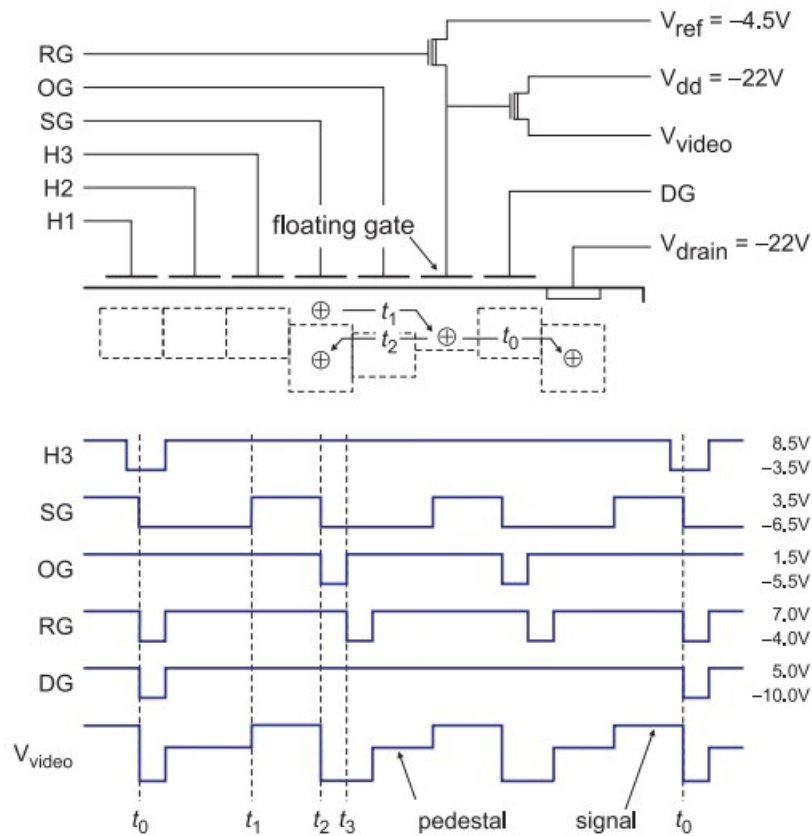


Figure 12: This image is an example of the different voltages needed for the operation of a skipper CCD. The lower scheme shows the video signal V_{video} as the sum of the clocks involved in the floating gate and in the serial clock in a CCD with subelectron noise [26]. In the upper side, it is shown the sequence of the charge moving by different gates.

If t_1 , t_2 and t_3 are repeated then a number of charge samples are obtained. To read the next pixel, the current charge is moved out from the CCD channel by resetting DG and RG pulse.

3.4.2 Background Performance

The key point in averaging the charge samples is that the measurements are uncorrelated therefore by taking the uncorrelated Gaussian readout noise, the standard deviation σ of the effective readout noise distribution after averaging N samples per pixel is given by [28]:

$$\sigma = \frac{\sigma_1}{\sqrt{N}} \quad (3)$$

where σ_1 is the standard deviation for one sample. The next figure plot the decreasing readout noise with the number of samples according with the equation 3.

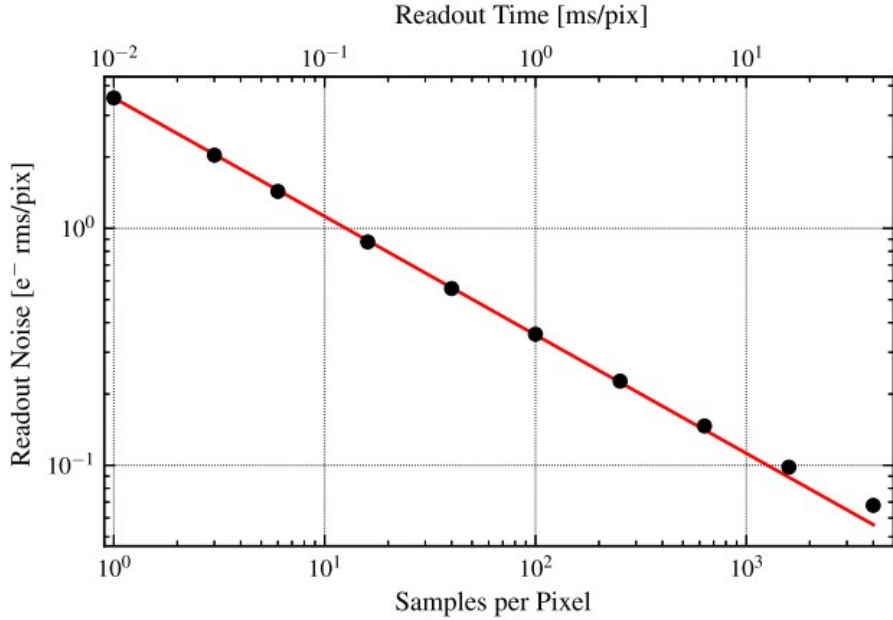


Figure 13: This plot shows how the readout noise is reduced by the number of charge samples (black points) and the theoretical expectation assuming independent and uncorrelated samples (red line) [28].

4 Test Chamber Setup for CCD's.

For the incoming years, the DAMIC-M collaboration will keep developing new CCDs technologies in order to accomplish a Kg size and reach a sub-electron noise detector which will be installed underground. In particular, as part of this collaboration, the Institute of Physics in Cantabria (IFCA, in spanish) is implementing new algorithms and characterization techniques for simulation and calibration for a new skipper CCDs generation.

To accomplish the target, the IFCA has obtained a very specialized equipment aiming to not introduce an external noise into CCD images and at the same time has devoted an almost isolated place inside the Clean Room to install a CCD test chamber which is been called as Ironman. The Clean Room facilities are intended to microelectronics manufacturing and scientific research so the quantity of dust and other pollutants is very low. Also in this facilities there is an access room of 6 square meters pressurized at +15 Pa. Moreover, According to ISO 14644, the Clean Room is class 5.5 and the access room is class 8 so assures a high confidence to perform measurements with the CCDs.

During the first semester of this year, a number of components of the Test Chamber have been installed together with the Slow Control and the LEACH system.

During this chapter, the setup for the Ironman test chamber, the Slow Control and the LEACH system are exposed with their features and different components. Furthermore, some plots on the Ironman performance are analyzed.

4.1 Cryostat

The main objective of the Ironman chamber is to produce the conditions for a good performance in the CCD components. The first condition is reach a temperature about 135 °K, this occurs trough the use of a cryostat which is in thermal contact with the upper side of the chamber. The second one is to maintain an environment free of condensation (due to low temperatures) that may affect the electronics inside the chamber this with the help of a Pumping Station.

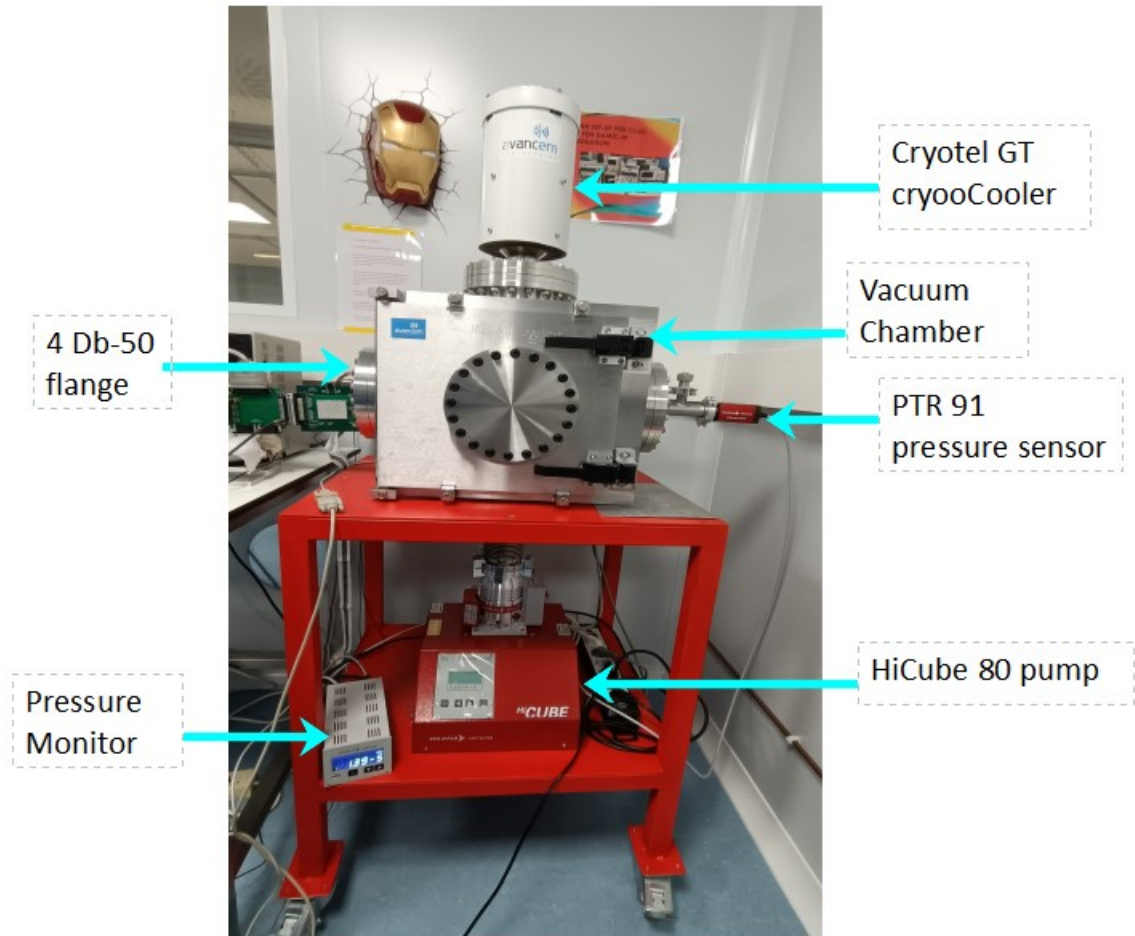


Figure 14: View of the main components of the Ironman Test Chamber. This setup is now installed in the Clean Room at IFCA.

As shown in the figure 14, a number of setup components are mounted on a metal aluminium structure. Fortunately, this structure has not shown to be a noise source. This structure is also equipped with wheels that facilitate the transport of the experiment.

The vacuum chamber is closed by a pair of handles, a pair of screws at the top and another pair at the bottom.

4.1.1 Equipment for Ironman

Apparatus	Model
Cryocooler	Cryotel GT
Vacuum Pump	HiCube 80
Temperature Controller	CTC 100
Pressure Monitor	PFEIFFER Vacuum CenterOne
Pressure Sensor	PFEIFFER PTR 91

The table above shows the main components for the Ironman chamber, all of them have a DC power supply of 220 V.

The most complex system in the Chamber setup is the cryogenic and it is going to be discussed later. To turn the Vacuum Pump on it is only necessary pushing the button on and the air will start to get out the chamber. A similar button applies to the pressure monitor and Cryogenic Temperature Control (CTC 100).

4.1.2 Cryogenic System

The target of the cryogenic system is to help with decreasing the temperature in a controlled way as well as stabilize the temperature inside the chamber ($\approx 135^\circ\text{K}$). The Cryotel GT is a free-piston, Stirling-cycle-based cryocooler that incorporates a cold finger, an internal piston and displacer, a pressure vessel, and a passive balancer, among other components, into one compact, integral unit. The linear alternator inside the pressure vessel converts electrical power from the controller into linear motion of the piston. The oscillating pressure wave generated by the piston passes from the pressure vessel into the cold finger causing the displacer inside the cold finger to move. The pressure wave and regenerator in the cold finger create a temperature difference which sets up a Stirling thermodynamic cycle which moves heat from the cold tip to the heat rejector resulting in a decreasing cold tip temperature (Information indicated by the manufacturer).

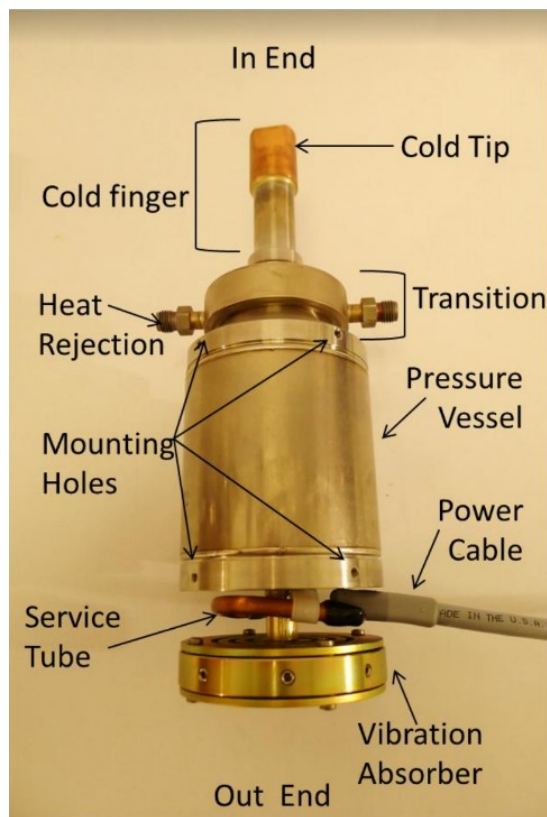


Figure 15: Main components of CryoTel GT cryocooler (Credits: SUN-POWER).

The Vibration Absorber (located in the Out end in figure 15) was replaced by a AVC balancer (provided by the manufacturer) connected to an Active Vibration Cancellation (AVC) system providing a significant active reduction of the exported cryocooler vibration by applying an equal force in the opposite direction of the cryocooler’s moving components.

The AVC system has a Controller dedicated to supply DC energy to the Cryocooler, measure the vibrations (with an accelerometer), provide instructions to the AVC balancer and communicate with the user trough an RS-232 serial port on a computer.

Operating the cryocooler in a default mode is been carried out by connecting the cryocooler controller to the computer by converting the serial

output to USB COM communication thus with a Putty terminal is send the line commands for operation.

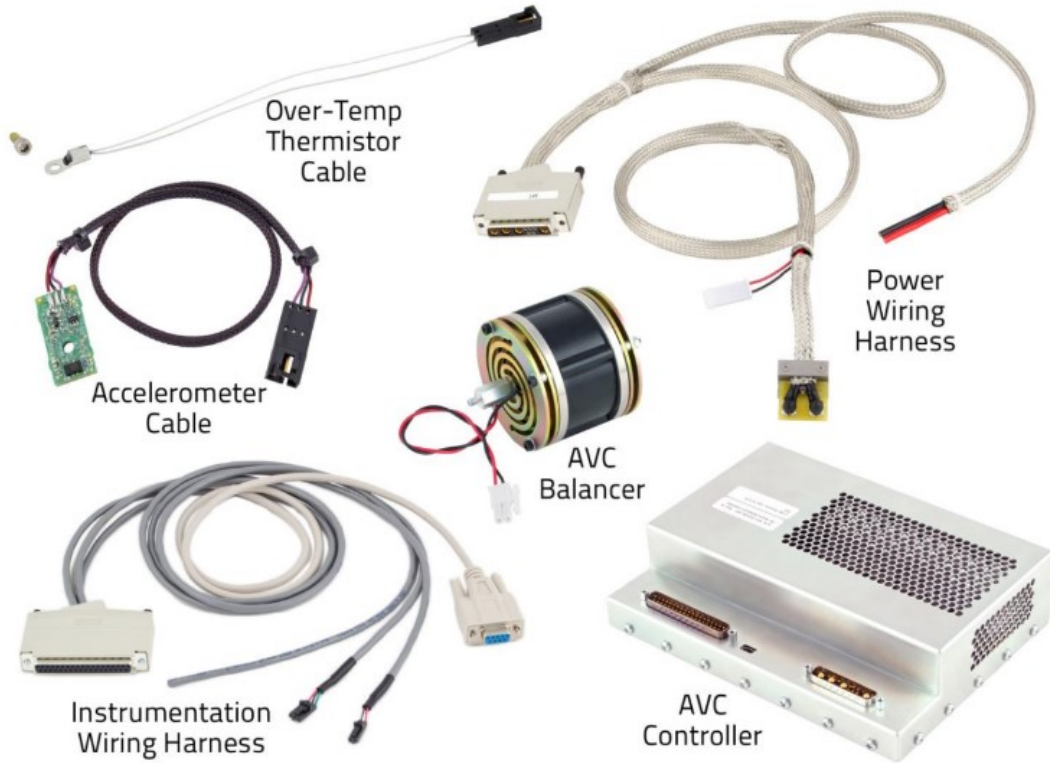


Figure 16: Elements in the AVC system.

Another feature of the is the Cryotel GT is reject over-temperature alarm. For this the Over-Temp thermistor Cable has to be connected between the AVC controller and cryocooler. Also the AVC controller can measure the temperature inside the vacuum chamber by using a PT100 temperature sensor.

An important part in the cryogenic system is the Cryogenic Temperature Controller (CTC100) which provides power to a heater installed inside the vacuum chamber. With a temperature sensor, a diode (25Ω) in thermal contact with the CCD receives from the CTC enough power to control the temperature gradient ($\approx 1^\circ\text{k}/\text{min}$) and stabilize the CCD temperature over a long period of time either to expose the CCD or be in standby.

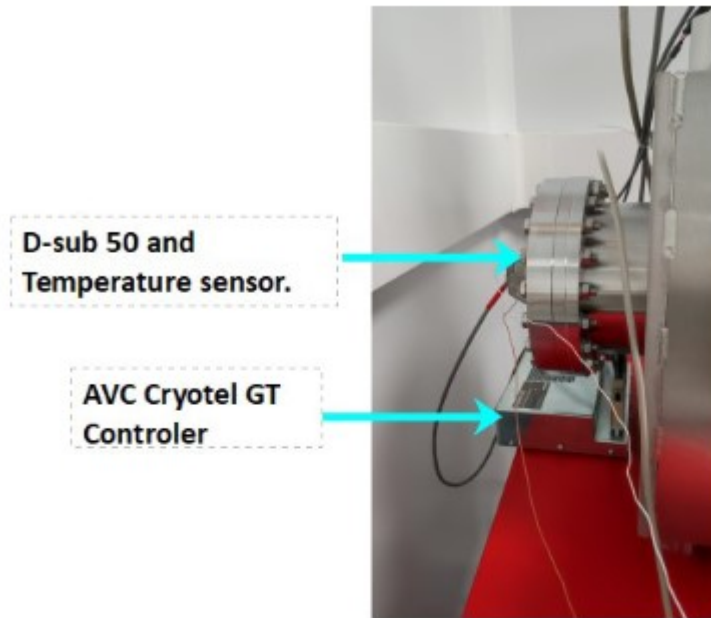


Figure 17: View of the back of the vacuum chamber.

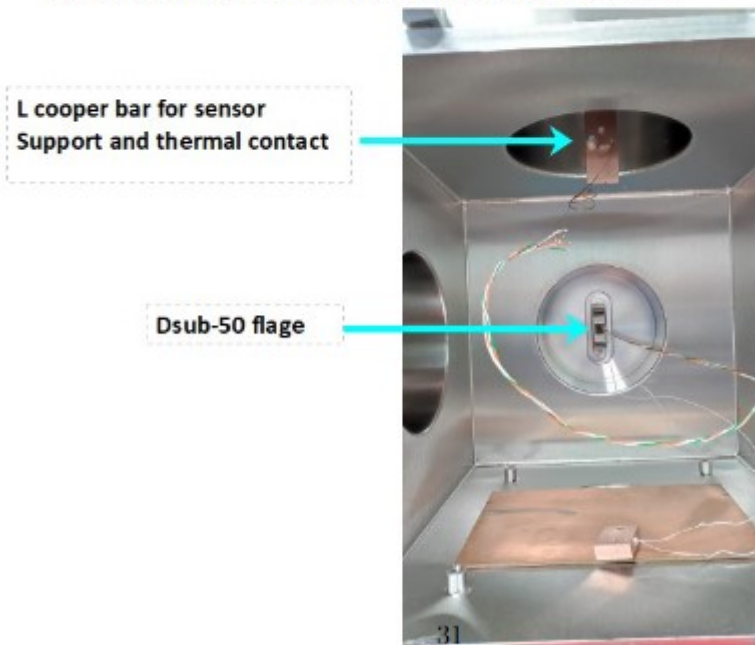


Figure 18: View inside of the vacuum chamber. There is a metal bar at the bottom to protect the duct between the pump and the vacuum chamber.

Inside of the vacuum chamber, the CCD is mounted on a metal base holding on a L cooper bar, the last one has some holes to keep either temperature sensors or heater diodes both from the CTC100.

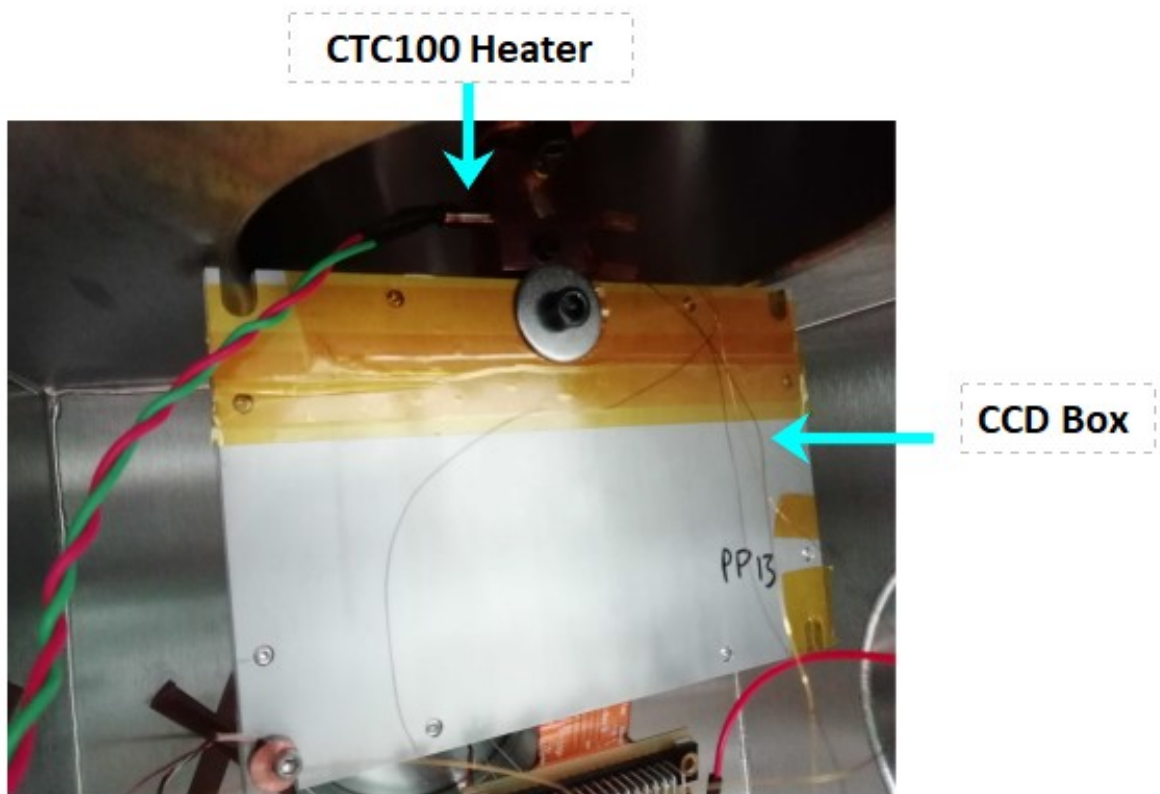


Figure 17: View of the CCD box installed inside the vacuum chamber. The temperature diode is installed on the L cooper bar just behind the CCD box.

4.1.3 Operation

After a series of attempts to keep the temperature gradient about 135° k, vacuum level and security warnings for the setup experiment. It is been proposed by the DAMIC- M collaboration to follow the next suggestions to operate the Ironman Test Chamber:

- If the vacuum chamber is going to be opened, the person has to ensure that the special metal plate must be collocated on the chamber base to avoid any accident with pump duct.
- When the chamber is going to be closed, the person must be sure to take the metal bar off the base.
- To manipulate any electronic device inside or outside the chamber, the person has to wear anti static gloves and bracelet.
- The preferred vacuum level to operate with a CCD must be below of 9.9×10^{-5} mbar.
- To have a successful parameters (PID are the parameters for the algorithm used to modulate the power provided by the CTC100 to the heater)) calculation with the Cryogenic Temperature Controller, the temperature inside the chamber has to be in thermal equilibrium with the environment and the cryocooler must be in standby.
- After the CTC calculate the parameters, the cryocooler must be set on with the maximum power and turn it on (pwout=135 y cooler=power in putty or with Slow Control).
- Wait until the vacuum pump is totally stopped (after turning it off it takes like 15 minutes to totally stop) to open the valve slowly.

4.1.4 Performance

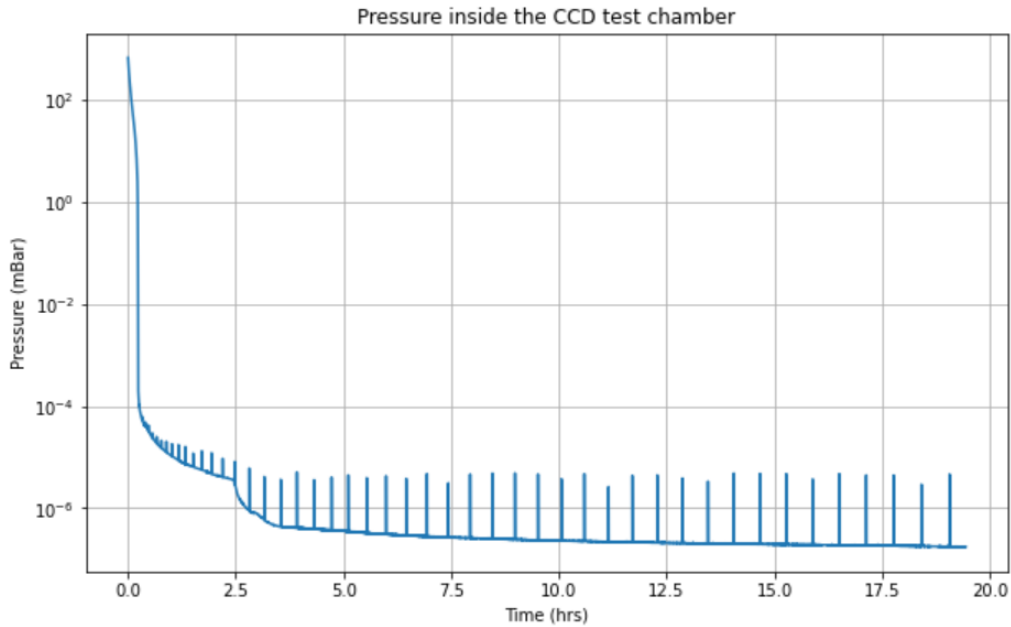


Figure 18: Plot of the Pressure inside the Ironman test chamber.

With the help of the CTC100, the PTR91 sensor and the monitor pressure it is possible to monitoring the temperature and pressure inside the vacuum chamber. For first measurements of this last two parameters, the vacuum chamber only contains the temperature and heater diodes inside aiming to test the well working of the test chamber. With this mind, in the figure 18 it is shown how the pressure changes with time, the vacuum is generated by taking the air off by the pumping station. In less than an hour the vacuum reached 10^{-5} mbar and takes about 2.5 hours to reach the desired vacuum level to operate the CCD. After that, the pressure keeps most of the time lower than 10^{-6} mbar with sporadic pressure peaks with values lower than 10^{-5} mbar.

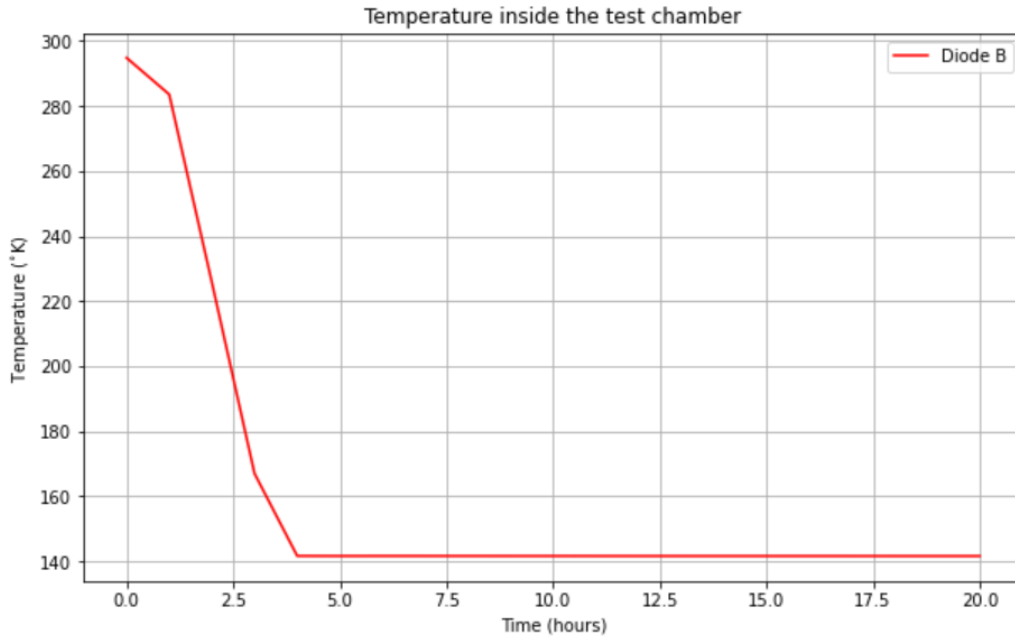


Figure 19: Plot temperature vs time.

In figure 19, the plot shows the behavior of the temperature inside the test chamber over time. In this case the temperature sensor is installed just behind the CCD box on the copper L type bar which ensures a high level thermal contact with the CCD. After the installation of the cryostat a number of test were performed in order to verify that the cryocooler system works as expected therefore from the plot we can identify 4 different slopes (by approximating the curve to straight lines) corresponding to four different stages to reach and keep the temperature in 141 ° K. The first stage goes from room temperature (293 ° K) to ≈ 283 ° K, it is a temperature decrease of about 10 degrees in one hour. For the second stage, the temperature goes from 283 to 163 Kelvin degrees in two hours which means that the temperature gradient is about 1 ° K per minute (the one needed for CCD operation). In case of the third stage, there is a change in temperature from 163 ° K to 141 ° K in just one hour afterwards in the last stage the temperature is almost constant in approximately 141 ° K with very slightly variations during at least 16 hours.

4.2 LEACH System

In the past chapters the readout functioning of a skipper CCD and the type of signals and bias necessary to operate it were introduced then this chapter presents some basics about the electronics to control the skipper CCD installed inside the cryostat. This electronics set is named as the LEACH system.

Some electronics used in the LEACH system at the Clean Room at IFCA was acquired to the Astronomical Research cameras, Inc. (ARC) with the objective to control the following items for the CCD readout operation: clock sequencing and delays, clock and bias voltages, image dimensions, pixel binning and system gain. The ARC devices are listed below:

- ARC-22, 250 Mhz Fiber Optic Timing Board.
- ARC-32, CCD Clock Driver Board.
- ARC-33, LBNL Bias Board.
- ARC-45, Two Channel CCD Video Board.
- ARC-66, PCI Interface Board.
- ARC-70, 6-Slot Closed Housing System.
- ARC-80, Large Power Supply.
- ARC-74, Fiber Optic Cable.
- ARC-82, Power Supply Cable.

In case of the timing, clock, and video boards they were installed in the 6-slot housing system (see figure 20). The PCI interface board is installed into the lab's computer. To verify that the connection between the Housing system and the PCI board is adequate the LEDs on either side of the housing system turn on green otherwise the LEDs turn on red.

The software used to control the LEACH system is the CCDDrone which is installed in the local computer. For a better compatibility between the



Figure 20: Image of the 6-Slot Closed Housing System with the corresponding installed boards, from left to right, the Fiber Optic Timing board, CCD Clock Driver and CCD Video board.

PCI board drivers and the computer the Centos8 operating system is used.

The main target actions to execute for the **ARC-22 250 MHz Fiber Optic Timing Board** are communicating between the controller and the local computer, generating timing waveform and providing overall controller supervision. With the ARC-74, operating at a bit rate of 250 MHz and having as a maximum image data transfer rate of 12.5 MP per second, a link between the PCI interface board and the timing board is established.

In case of the **ARC-32 CCD Clock Driver Board** its duty is translate

the input signals into analog output signals for direct connection to CCD. It provides 24 clock signals and will drive up to ± 13 V for operating CCD arrays.

For the **ARC-45 Two Channel CCD Video Board**, it has to process and digitize video outputs from two CCD video channels and supply DC bias voltages to the CCD through external power sources. It has two 16-bit analog-to-digital converters that digitize signals from two video outputs. The DC bias provides ten low noise voltage outputs suitable for direct connection to CCDs.

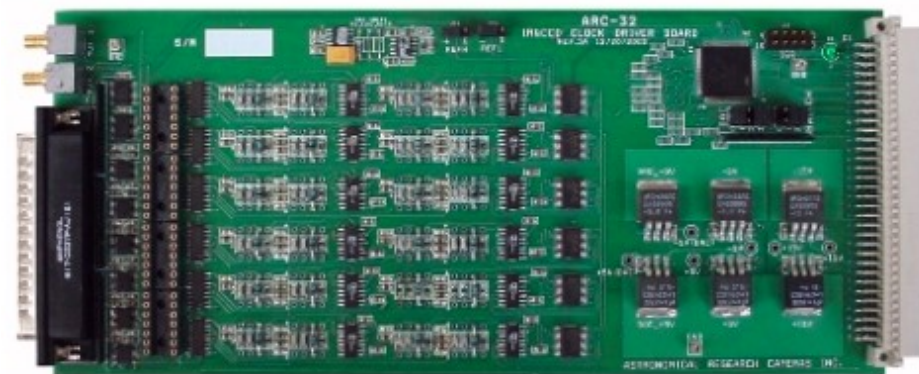
The communication and data transfer between the local computer and the controller is carried out by the **ARC-66 PCI Interface Board** this via a fiber optic cable connection with a maximum sustained data transfer of 12.5 MP/second.



Figure 21: The ARC-66 PCI Interface Board



(a) The ARC-22 250 Mhz Fiber Optic Timing Board.



(b) The ARC-32 CCD Clock Driver Board.



(c) The ARC-45 Two Channel CCD Video Board.

The Leach PCB breakout board is installed outside the vacuum chamber and connected to the 4 Db-50 flange. It is on charge of providing the different bias voltages to the skipper CCD, for each V_{ref} , V_{dd} and V_{drain} voltages (CCD bias) a SMA connector supply the power. Also, this board is connected to the Clock and Video boards. In the figure 23, the second stage board (right) contains the CCD amplifiers which increase enough the collected charge in order to digitize its signal. Another SMA connector provides the power to the operational amplifiers which is ± 5 V.

For the substrate depletion voltage V_{sub} is used an external low noise source SRS DC205 that communicates with the local PC via RS323 computer interface and the CCDDrone program.

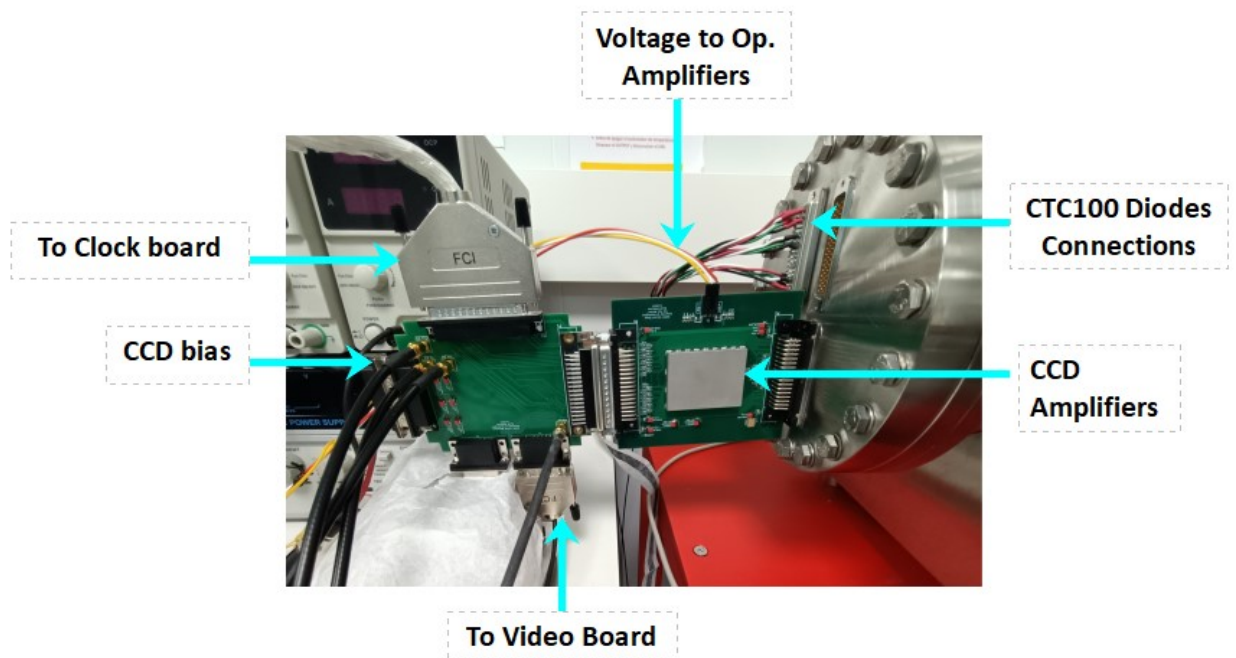
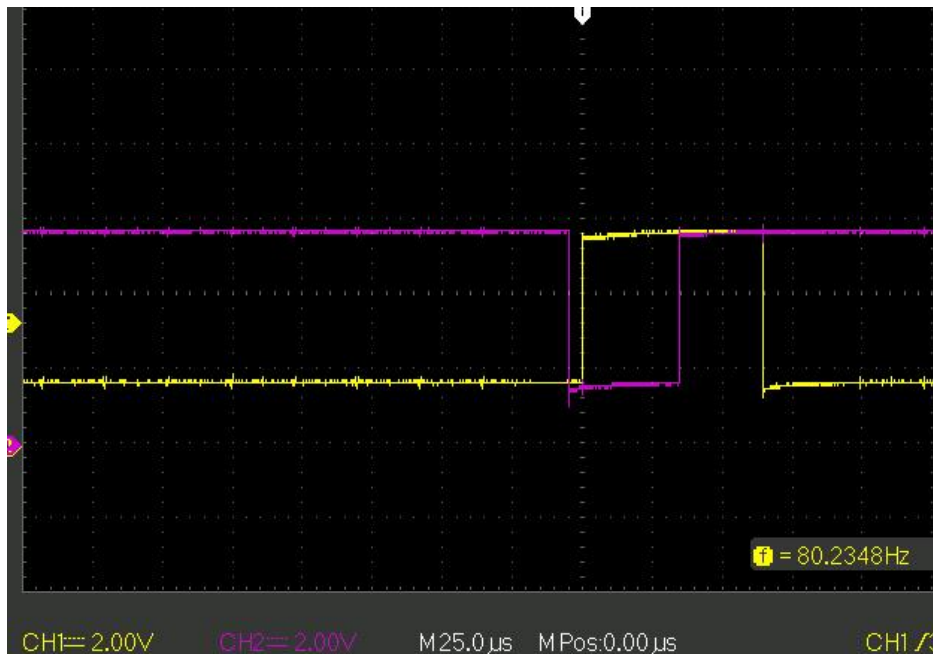
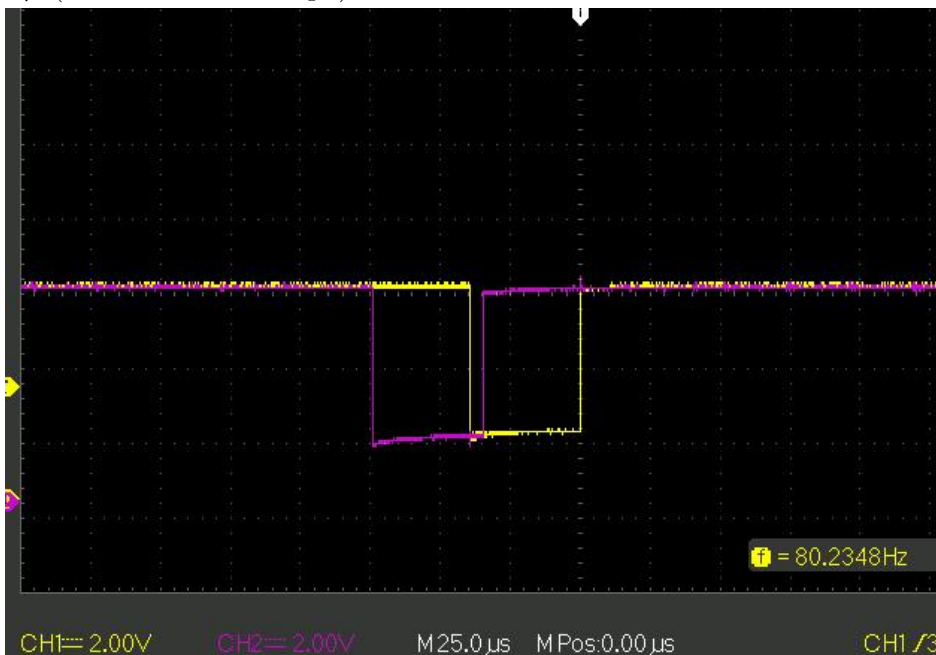


Figure 23: This picture show the connection in the Leach PCB breakout (left) and seconds stage board (right).

To verify the LEACH system is working as expected then a number of measurement s for the signal clocks was made by taking the signal from the clocks board with an oscilloscope. The next images are showing the overlay of different signal clocks which have the same amplitude equal to 2 V.



(a) Parallel Clocks. Overlay of V1 and V2 waveforms with an overlap of 5μ (Credits: Julia Campa).



(b) Parallel Clocks. Overlay of V1 and V3 waveforms with an overlap of 5μ (Credits: Julia Campa).

4.3 Slow Control

Aiming to monitoring and having access to the main components of the CCD test Chamber while the scientist are outside the Clean Room the design and installation of a Slow Control (SC) was carried out. Trough this section the characteristics, software and hardware implemented in the Slow Control are presented.

This SC was based on the implemented one for the CCD Test chamber in The University of Chicago and on the astro-slow-control package by J. Nikkel (Yale) then some modifications were made to the source code to adapt it to the needs of the experimental setup at IFCA. The SC uses the TPC/IP protocol to communicate devices with a server mounted on the local computer inside the Clean Room trough a physical network.

4.3.1 Software

To accomplish the target of the Slow Control, it is necessary to use a HTTP web server, a database administrator, a dedicated Operating System and a programming language to develop web interfaces. To satisfy the compatibility with the Slow Control scripts for the University of Chicago the next software versions were installed:

- Maria Database.
- PHP 5.1 (web programimng language).
- Centos8 (Linux distribution).
- Apache (web server).

The software above is called as the LAMP stack. The **backend** is dedicated to the control libraries for each instrument that we want to communicate with. For the **frontend** a user interface is displayed on the web browser to control the instruments.

The SC also provides the option to control the users and their access to perform duties with the connected devices. In the case of root users they can control the permissions for another user, access to data monitoring as well as add a new device to the Slow Control. For gest users they only have access to data monitoring for the cryogenic temperature controller.

After mounting the web server, a data base provided by Danielle Norcini (The University of Chicago) was used to have compatibility with the user interface. This database named as **Control** have the fields to store data related to users, access time, data taken from the CTC, the installed devices and their IP address. If the person who want to access to the SC for just monitoring data then no password is required but if the user want to make some changes to SC, for instance, adding a new device, turn on or turn off some apparatus then a password is needed.

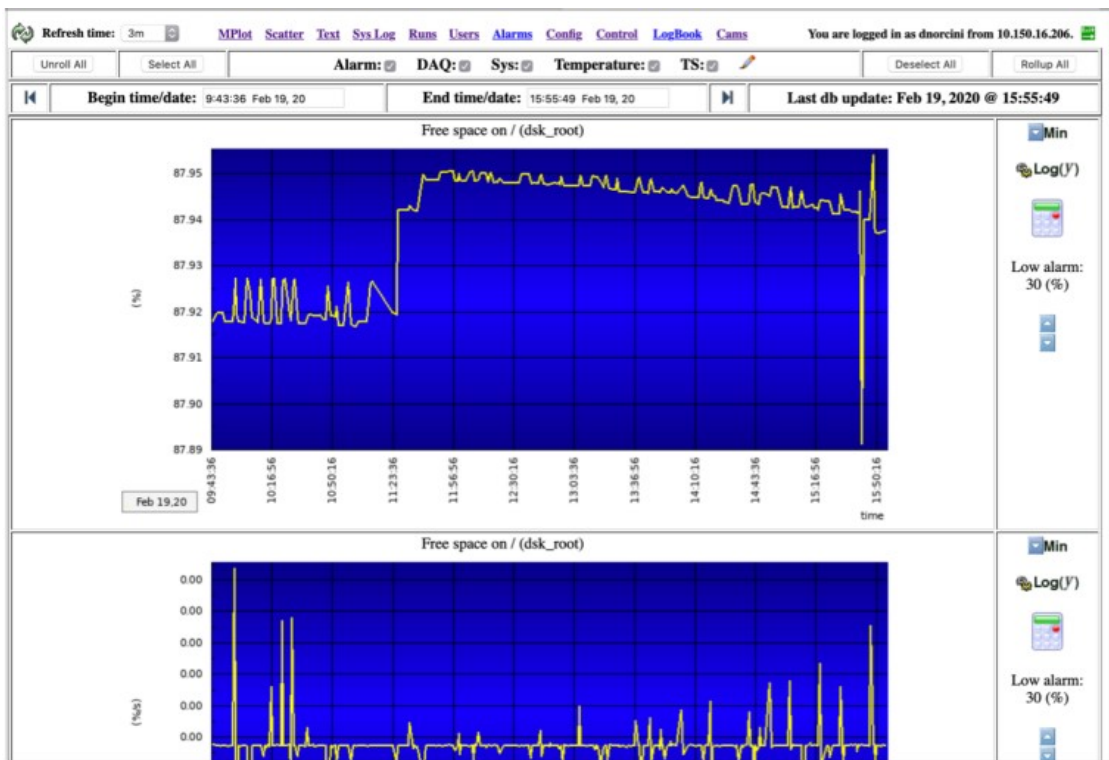


Figure 25: Image of the Data monitoring from the free space on disk with the Slow Control interface.

Almost all backend and frontend software have been uploaded to the Danielle Norcini github repository [1]. The controllers for each device connected to SC are written in C then it is necessary to compile all of them. The user interface is coded in PHP and it is necessary to upload the source code on the Apache web server and do all the enough modifications according to the network and hardware architecture. To get into the SC interface the user

must write in the web browser: `http://localhost/SC_web/index.php` and decide which kind of session (guess or registered) wants to start.

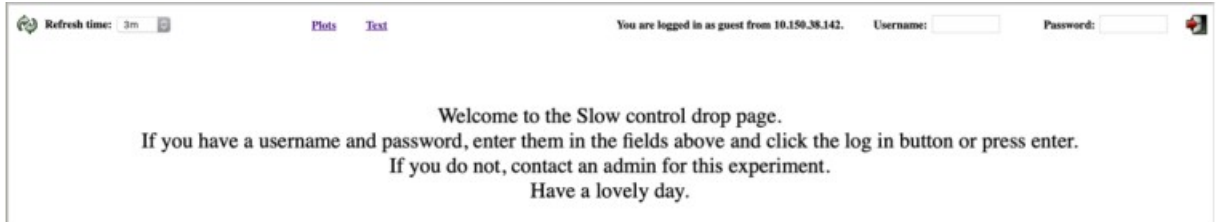


Figure 26: Login page to SC.

4.3.2 Hardware

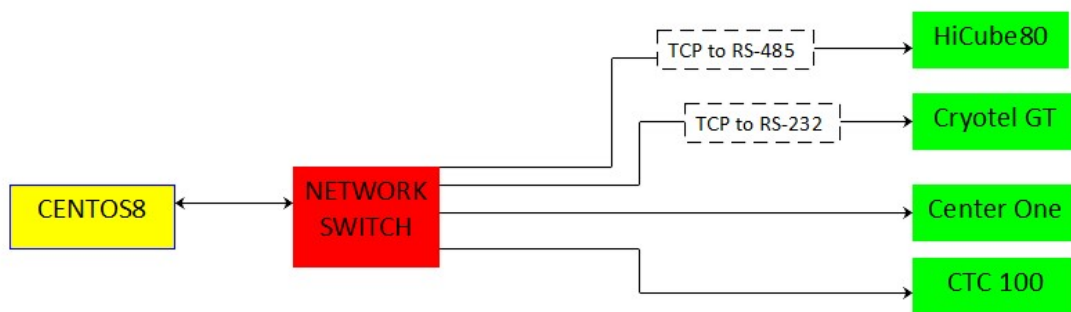
One good feature of almost all devices used so far is that they have a number of ports to communicate with PC (either via Ethernet or serial connection) or store data in an external disk. To have a better Ethernet administration, a Network Switch (NS) is set inside the Clean Room to configure all the physical connections between the devices and the server. Furthermore, the devices added to the SC as well as the type of connection are listed below:

- HiCube 80 (the vacuum pump): It is necessary to convert serial communication to TCP/IP. This is possible by using a coupling device (PM 061 270 -X) from M12 to RS-485 then through a serial to Ethernet converter (Perle) a communication link between the Network Switch and the pump is established. Nevertheless, when the user tries to ping with the HiCube 80 device there is still no response.
- Cryotel GT: In case of the cryocooler, also it is necessary to convert serial (RS-232) to TCP/IP communication cable. The communication is established between the cryocooler controller and a serial-to-Ethernet converter (StarTech).
- CenterOne: This pressure monitor works with an Ethernet port therefore it is only about to make a connection between the apparatus and the Network Switch.
- CTC100: Also this apparatus has an Ethernet port and the connection is directly with the NS.



(a) Switch Network device connected to the Ethernet network.

Slow Control schematic for Ironman



(b) Schematic for the Slow Control connections and devices.

5 First skipper CCD images at IFCA

After installation of most of the CCD test chamber components a number of tests have been carried out in order to verify its functionality. Then it is a good idea to verify if the cryostat produces the enough good conditions to observe some particles coming from atmospheric showers or some radiation source inside the Clean Room. Furthermore, in this chapter I introduce the first CCD images taken in the IFCA's Clean Room with some observation on the particles detected.

The first used CCD is PP13-U which only operates with one amplifier **U**, the pixel size is $15\mu m \times 15\mu m$ with resolution 6000×1500 . For the taken image in figure 28 the charge moves to amplifier **U** at 135°K , the integral time is $10 \mu s$ and the depletion voltage $V_{sub} = 45 \text{ V}$. The bias and clocks voltages used are listed in the next table:

Signal	(V)
V1	1.5-4.0
V2	1.5-4.0
V3	1.5-4.0
H1	-0.5-2.5
H2	-0.5-2.5
H3	-0.5-2.5
TG	1.5-4.0
OG	-9.0, -4.0
SW	-9.0, -3.0
DG	-8, -4
V_{dd}	-22.0
V_{drain}	-22.0
V_{reff}	-7.0

Table 1: Clock and bias Voltages values.

By following the criteria that muons from cosmic rays are minimum ionising particles and go through the detector following straight lines, while energetic electrons produced by electromagnetic radiation draw small curved tracks [37] I do an identification of electrons and muons for some tracks in the CCD image.

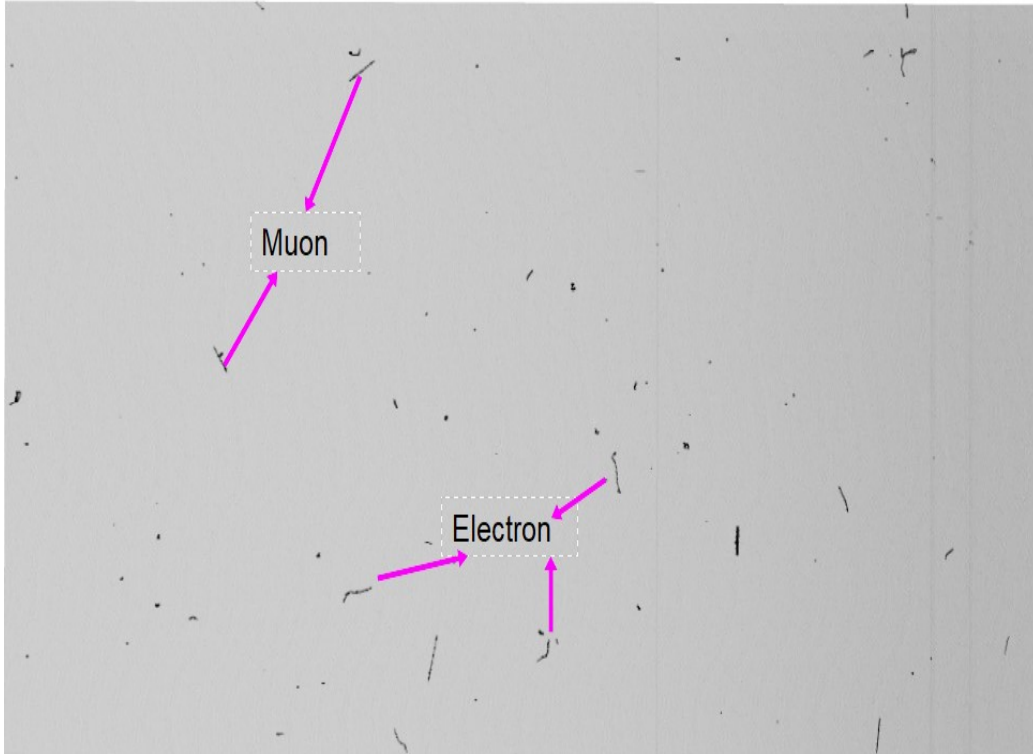
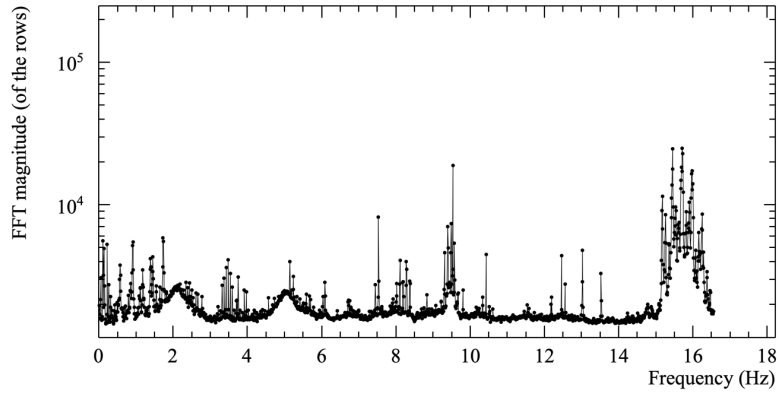


Figure 28: This figure shows the particle identity for some tracks in the CCD image (Credits: Rocio and Nuria).

The next test was carried out with the CCD PP52 which only operates with two amplifiers **U** and **L**, the pixel size is $15\mu m \times 15\mu m$ with resolution 6000×1500 is measure the noise in the serial register which means no transporting the collected charge in the pixels to the amplifiers, for this the integration time is set in $5 \mu s$ with $V_{sub} = 45 V$ at $135^\circ K$ with the rest parameters value shown in the table 1.

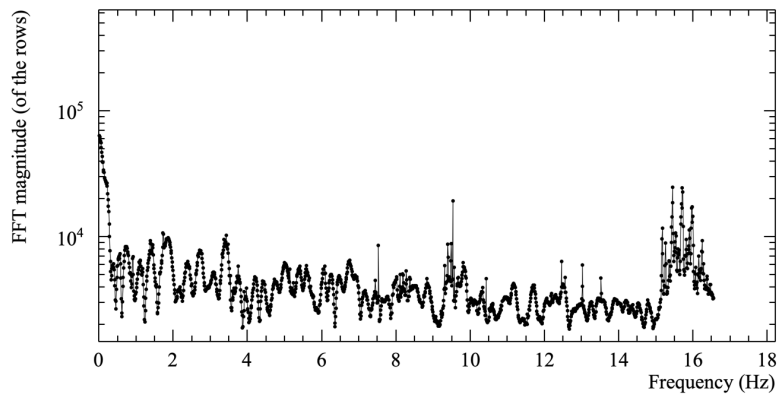
The next two plots shows the FFT magnitude of the CCD rows. A good CCD with very low noise will have the plot almost flat. For the amplifier **U** we can see there are several peaks with the bigger one at higher frequencies and we observed the same for the amplifier **L** although its graph is more flatten.

[amplifier U]



(a) Plot of the FFT magnitude for the U amplifier.

[amplifier L]



(b) Plot of the FFT magnitude for the L amplifier.

6 Conclusions

From the graphs on pressure and temperature inside the vacuum chamber over time, the behavior of the cryogenic system is as expected. In the case of the pressure it takes at least one hour to reach the optimal level vacuum to operate the CCD at less than 10^{-5} mbar then the vacuum level remains almost constant for a long time this suggest that there is not a significant air entrance nor a gas production inside. For the temperature, we observed how the slope remains constant while the chamber inside is getting cooler this means a good performance of the Cryogenic Temperature Controller in providing power to the heater and that it is capable to keep the temperature constant at very low temperatures for a long period of time.

The LEACH system hardware provides with high accuracy the signal clocks to the CCD as well as the readout of the pixels charge this is seen in the clocks signal images and the image of the traces of muons and electrons formed by the readout operation of the CCDs.

The Slow Control system is working well for all the devices except for the HiCube 80 pumping station that is not having communication via TCP/IP protocol with the local computer, a possible issue is that the serial signal is not well converted to Ethernet output.

It is not possible to explain the noise source in the serial register yet because the significantly different plots profile with each of the amplifiers, U and L and there isn't any noise patron. A further duty will be to isolate electrically the pumping station, measure the noise levels again, test the cables in Ironman and study the noise levels over the integration time.

7 Bibliography

References

- [1] Trimble, V. (1987). Existence and nature of dark matter in the universe. *Annual review of astronomy and astrophysics*, 25(1), 425-472.
- [2] Lee, S. J., Kilminster, B., and Macchiolo, A. (2020). Dark Matter in CCDs at Modane (DAMIC-M): a silicon detector apparatus searching for low-energy physics processes. *Journal of Instrumentation*, 15(02), C02050.
- [3] Zwicky, F. (1933). The redshift of extragalactic nebulae. *Helvetica Physica Acta*, 6, 110-127.
- [4] Freeman, K. C. (1970). On the disks of spiral and S0 galaxies. *The Astrophysical Journal*, 160, 811.
- [5] Rubin, V. C., and Ford Jr, W. K. (1970). Rotation of the Andromeda nebula from a spectroscopic survey of emission regions. *The Astrophysical Journal*, 159, 379.
- [6] Rubin, V. C., Ford Jr, W. K., and Thonnard, N. (1978). Extended rotation curves of high-luminosity spiral galaxies. IV-Systematic dynamical properties, SA through SC. *The Astrophysical Journal*, 225, L107-L111.
- [7] F. Dyson, A. Eddington, and C. Davidson, "A Determination of the Deflection of Light by the Sun's Gravitational Field, from Observations Made at the Total Eclipse of May 29, 1919", *Philosophical Transactions of the Royal Society of London* 220 (1920), 291–333.
- [8] Wambsganss, J. (1998). Gravitational lensing in astronomy. *Living Reviews in Relativity*, 1(1), 1-74.
- [9] Einstein, A. (2005). Die Grundlage der allgemeinen relativitätstheorie [AdP 49, 769 (1916)]. *Annalen der Physik*, 14(S1 1), 517-571.
- [10] Ofek, E. O., Rix, H. W., and Maoz, D. (2003). The redshift distribution of gravitational lenses revisited: Constraints on galaxy mass evolution. *Monthly Notices of the Royal Astronomical Society*, 343(2), 639-652.

- [11] Massey, R., Kitching, T., and Richard, J. (2010). The dark matter of gravitational lensing. *Reports on Progress in Physics*, 73(8), 086901.
- [12] Ellis, R. S. (2010). Gravitational lensing: a unique probe of dark matter and dark energy. *Philosophical Transactions of the Royal Society A: Mathematical, Physical and Engineering Sciences*, 368(1914), 967-987.
- [13] Massey, R., Rhodes, J., Leauthaud, A., Capak, P., Ellis, R., Koekemoer, A., ... and Van Waerbeke, L. (2007). COSMOS: three-dimensional weak lensing and the growth of structure. *The Astrophysical Journal Supplement Series*, 172(1), 239.
- [14] CL Bennett, WMAP observations: Final maps and results. *Astrophys J Suppl Ser* 208, 20–73 (2013).
- [15] Planck Collaboration; Ade PAR, et al. (2014) Planck 2013 results: I. Overview of products and scientific results. *Astron Astrophys* 571:1–48.
- [16] Karmakar, S., Singh, M. K., Singh, V. (2021, June). Current status of different detector technology in the searches of dark matter events. In *Journal of Physics: Conference Series* (Vol. 1947, No. 1, p. 012009). IOP Publishing.
- [17] Roszkowski, L., Sessolo, E. M., Trojanowski, S. (2018). WIMP dark matter candidates and searches—current status and future prospects. *Reports on Progress in Physics*, 81(6), 066201.
- [18] Feng, J. L. (2010). Dark matter candidates from particle physics and methods of detection. *Annual Review of Astronomy and Astrophysics*, 48, 495-545.
- [19] <https://damic.uchicago.edu/detector.php>
- [20] Janesick, J. (1987). Sky on a chip: the fabulous CCD. *Sky and Telescope*, 9, 238-242.
- [21] Mackay, C. D. (1986). Charge-coupled devices in astronomy. *Annual review of astronomy and astrophysics*, 24, 255-283.
- [22] Chavarria, A. E., Tiffenberg, J., Aguilar-Arevalo, A., Amidei, D., Bertou, X., Cancelo, G., ... & Zhou, J. (2015). Damic at snolab. *Physics Procedia*, 61, 21-33.

- [23] Holland, S. E., Groom, D. E., Palaio, N. P., Stover, R. J., & Wei, M. (2003). Fully depleted, back-illuminated charge-coupled devices fabricated on high-resistivity silicon. *IEEE Transactions on Electron Devices*, 50(1), 225-238.
- [24] Janesick, J. R., Elliott, T., Collins, S., Blouke, M. M., & Freeman, J. (1987). Scientific charge-coupled devices. *Optical Engineering*, 26(8), 692-714.
- [25] Howell, S. B. (2006). *Handbook of CCD astronomy* (Vol. 5). Cambridge University Press.
- [26] Fernández Moroni, G., Estrada, J., Cancelo, G., Holland, S. E., Paolini, E. E., & Diehl, H. T. (2012). Sub-electron readout noise in a Skipper CCD fabricated on high resistivity silicon. *Experimental Astronomy*, 34(1), 43-64.
- [27] Wen, D. D. (1974). Design and operation of a floating gate amplifier. *IEEE Journal of Solid-State Circuits*, 9(6), 410-414.
- [28] Tiffenberg, J., Sofu-Haro, M., Drlica-Wagner, A., Essig, R., Guardincerri, Y., Holland, S., ... & Yu, T. T. (2017). Single-electron and single-photon sensitivity with a silicon Skipper CCD. *Physical review letters*, 119(13), 131802.
- [29] McLean, I. S. (2008). *Electronic imaging in astronomy: detectors and instrumentation* (Vol. 552). Berlin: Springer.
- [30] DAMIC collaboration, and de Mello Neto, J. R. T. (2016). The DAMIC dark matter experiment. *PoS (ICRC2015)*, 1221.
- [31] Aguilar-Arevalo, A., Amidei, D., Bertou, X., Bole, D., Butner, M., Cancelo, G., ... and Zhou, J. (2015). Measurement of radioactive contamination in the high-resistivity silicon CCDs of the DAMIC experiment. *Journal of Instrumentation*, 10(08), P08014.
- [32] J. Barreto et al. [DAMIC Collaboration], Direct search for low mass dark matter particles with CCDs, *Phys. Lett. B* 711 (2012), no. 3-4 264269 [arXiv:1105.5191]

- [33] Aguilar-Arevalo, A., Amidei, D., Bertou, X., Butner, M., Canelo, G., Vázquez, A. C., ... and Damic Collaboration. (2017). First direct-detection constraints on eV-scale hidden-photon dark matter with DAMIC at SNOLAB. *Physical review letters*, 118(14), 141803.
- [34] <http://www.lsm.in2p3.fr/>
- [35] Amare, J., Castel, J., Cebrián, S., Coarasa, I., Cuesta, C., Dafni, T., ... and Villar, P. (2018). Cosmogenic production of tritium in dark matter detectors. *Astroparticle Physics*, 97, 96-105.
- [36] Barak, L., Bloch, I. M., Cababie, M., Canelo, G., Chaplinsky, L., Chierchie, F., ... and Sensei Collaboration. (2020). Sensei: Direct-detection results on sub-gev dark matter from a new skipper ccd. *Physical Review Letters*, 125(17), 171802.
- [37] Tiouchichine, E., Haro, M. S., Bertou, X., Arnaldi, H., Berisso, M. G., Blostein, J., ... Moroni, G. F. (2017, July). Setup and Calibration of a particle detector based on Charge Coupled Devices. In *2017 Argentine Conference of Micro-Nanoelectronics, Technology and Applications (CAMTA)* (pp. 5-9). IEEE.